

# Non-exponential decay in quantum field theory and in quantum mechanics: the case of two (or more) decay channels

Francesco Giacosa

*Institut für Theoretische Physik, Johann Wolfgang Goethe - Universität  
Max von Laue-Str. 1, D-60438 Frankfurt am Main, Germany*

October 12, 2018

## Abstract

We study the deviations from the exponential decay law, both in quantum field theory (QFT) and quantum mechanics (QM), for an unstable particle which can decay in (at least) two decay channels. After a review of general properties of non-exponential decay in QFT and QM, we evaluate in both cases the decay probability that the unstable particle decays in a given channel in the time interval between  $t$  and  $t + dt$ . An important quantity is the ratio of the probability of decay into the first and the second channel: this ratio is constant in the Breit-Wigner limit (in which the decay law is exponential) and equals the quantity  $\Gamma_1/\Gamma_2$ , where  $\Gamma_1$  and  $\Gamma_2$  are the respective tree-level decay widths. However, in the full treatment (both for QFT and QM) it is an oscillating function around the mean value  $\Gamma_1/\Gamma_2$  and the deviations from this mean value can be sizable. Technically, we study the decay properties in QFT in the context of a superrenormalizable Lagrangian with scalar particles and in QM in the context of Lee Hamiltonians, which deliver formally analogous expressions to the QFT case.

## 1 Introduction

The study of unstable particles is a basic subject of both nuclear and particle physics. The fact that the so called survival probability, i.e. the probability  $p(t)$  that an unstable state  $S$  formed at the time  $t = 0$  did not decay at the instant  $t > 0$ , does not follow an exponential decay law for short times is now theoretically [1, 2, 3, 4, 5, 6] and experimentally [7, 8, 9] established in the framework of quantum mechanics. Moreover, oscillations on top of the exponential function can also occur in the short time regime and could eventually last long enough to be detected [10, 11]. Also at very large times deviations take place: a power law, and not an exponential law, is realized [1].

In particular, in Ref. [4] the deviation from the exponential decay law has been described in the nonrelativistic quantum mechanical context of Lee Hamiltonians [12, 13]: this approach allows to mimic non-relativistic quantum field theory by including a continuum of states. In Refs. [14, 15] these deviations have been demonstrated in the framework of a genuinely (superrenormalizable) relativistic quantum field theoretical Lagrangian. Both approaches give rise to qualitative similar deviations from an exponential decay law in the short-time regime and also show an indication of oscillations afterwards.

In this work we study the decay of an unstable particle when more than one decay channel is present, both in the context of relativistic quantum field theory (QFT) and quantum mechanics (QM). This parallel allows also to show the formal similarities of these two approaches. The equations presented in this work are general and do not depend on the particular employed model(s). However, it is useful for a clear presentation to work with a well-defined theoretical setup: in QFT we employ, in line with Refs. [14, 15], scalar fields, which are free from spin complications, in the framework of a superrenormalizable relativistic Lagrangian. In the case of QM we employ Lee Hamiltonians (LH): we generalize the work of Refs. [4] in order to describe the decay of an unstable state into two distinct channels.

When (at least) two decay channels are present, one has to determine (both in QFT and in QM) the probability of decay in each channel. Namely, the aim is to calculate (to our knowledge for the first time) the decay probability that the unstable particle  $S$  decays in the  $i$ -th channel between the time interval  $t$  and  $t + dt$ . Each partial decay probability deviates from the corresponding Breit-Wigner limit. In this context an important quantity under study in the two-channel case is the ratio between the decay probability in the first channel over the decay probability in the second channel. While this quantity is constant in the usual Breit-Wigner (BW) limit and is equal to the ratio  $\Gamma_1/\Gamma_2$ , where  $\Gamma_1$  and  $\Gamma_2$  are the tree-level decay widths in the first and the second channel respectively, this is not true in the general case. There are time intervals in which the ratio of probabilities is larger than  $\Gamma_1/\Gamma_2$ , meaning that the decay probability into the first channel is enhanced. Vice-versa, there are time intervals in which the ratio is smaller than  $\Gamma_1/\Gamma_2$ , implying that the decay probability into the second channel is enhanced.

One of the main purposes of this paper is a general and theoretically based presentation of the equations related to the decay probability in each decay channel as function of time. For this reason we do not refer here to any particular physical system, but we keep the presentation as general as possible. Yet, in order to improve the understanding of the manuscript we shall present in the QFT case several plots of the introduced functions for a selected numerical example. Although the employed superrenormalizable QFT model is clearly not the most general QFT treatment, the form and the structure of the equations are quite general and could be easily extended to other more complicated and realistic QFT approaches.

The paper is organized as follows: In Sec. 2 we give an overview of the QFT formalism for the description of the decay of an unstable particle. We introduce a (superrenormalizable) Lagrangian density and discuss the relevant properties of the survival probability  $p(t)$ . In Sec. 3 we turn to the QM study of decays: to this end we introduce the Lee Hamiltonian, which shows a formally very similar behavior to the QFT case of Sec. 2. We review the most important equations in this approach and also present a relativistic generalization of it. In Sec. 4 we turn back to QFT and discuss in detail the formulae for the two-channel case, with special attention to the decay probability in each channel. For sake of clarity we concentrate on the case in which two decay channels are available; the generalization to  $n$  decay channels is straightforward and is presented in Appendix B. In QFT the expressions of the decay probabilities in each channel cannot be analytically derived in the most general case; to circumvent this problem, a ‘conjecture’ about the form of the solution is put forward. It is then shown that the conjectured solution fulfills all the necessary requirements. A numerical study of these solutions is presented, in order to show differences from the usual exponential limit. In Sec. 5 we study the same problem of the two-channel decay in QM with the help of Lee Hamiltonians: in this case it is possible to derive the exact expressions for the decay probabilities in a given channel and we can test the validity of the conjecture presented in the QFT case: a numerical study shows a very good agreement of the exact results with the proposed solutions for both the nonrelativistic and relativistic treatments of the Lee Hamiltonians. Finally, in Sec. 6 we briefly present our conclusions and outlooks.

## 2 General properties of decays in quantum field theory

### 2.1 A simple Lagrangian to study the two-channel problem

We introduce a relativistic (superrenormalizable) Lagrangian with the three scalar fields  $S$ ,  $\varphi_1$  and  $\varphi_2$ :

$$\mathcal{L} = \frac{1}{2}(\partial_\mu S)^2 - \frac{1}{2}M_0^2 S^2 + \frac{1}{2}(\partial_\mu \varphi_1)^2 - \frac{1}{2}m_1^2 \varphi_1^2 + \frac{1}{2}(\partial_\mu \varphi_2)^2 - \frac{1}{2}m_2^2 \varphi_2^2 + g_1 S \varphi_1^2 + g_2 S \varphi_2^2. \quad (1)$$

For definiteness, we assume that  $m_1 < m_2$ . The interaction terms  $g_1 S \varphi_1^2$  and  $g_2 S \varphi_2^2$  induce the decay processes  $S \rightarrow \varphi_1 \varphi_1$  and  $S \rightarrow \varphi_2 \varphi_2$ , see the pictorial representation in Fig. 1, panel (a).

It is useful to introduce the tree-level decay function as

$$\Gamma^{\text{t-1}}(x, m, g) = \frac{\sqrt{\frac{x^2}{4} - m^2}}{8\pi x^2} (\sqrt{2}g)^2 \theta(x - 2m) , \quad (2)$$

where  $\theta(x)$  is the step function and  $x$  plays the role of the ‘running’ mass of the unstable state  $S$ . The tree-level decay functions in the first and the second channel read respectively

$$\begin{aligned} \Gamma_{S\varphi_1\varphi_1}^{\text{t-1}}(x) &= \Gamma^{\text{t-1}}(x, m_1, g_1) = \frac{\sqrt{\frac{x^2}{4} - m_1^2}}{8\pi x^2} (\sqrt{2}g_1)^2 \theta(x - 2m_1) , \\ \Gamma_{S\varphi_2\varphi_2}^{\text{t-1}}(x) &= \Gamma^{\text{t-1}}(x, m_2, g_2) = \frac{\sqrt{\frac{x^2}{4} - m_2^2}}{8\pi x^2} (\sqrt{2}g_2)^2 \theta(x - 2m_2) . \end{aligned} \quad (3)$$

Similarly, we also introduce the total tree-level decay function as

$$\Gamma_S^{\text{t-1}}(x) = \Gamma_{S\varphi_1\varphi_1}^{\text{t-1}}(x) + \Gamma_{S\varphi_2\varphi_2}^{\text{t-1}}(x) . \quad (4)$$

The partial tree-level decay rates –as calculated from the Lagrangian (1)– are naively obtained by setting  $x = M_0$  into Eqs. (3). However, care is needed: as shown in the next subsection, the mass of the unstable particle  $S$  is modified by quantum fluctuations<sup>1</sup> (it is typically shifted to lower values):

$$M_0 \rightarrow M . \quad (5)$$

For this reason the on-shell tree-level expressions  $\Gamma_1$  and  $\Gamma_2$  for the partial decay widths are not evaluated at  $M_0$ , but at the physical value  $M$ :

$$\Gamma_1 = \Gamma_{S\varphi_1\varphi_1}^{\text{t-1}}(x = M) \text{ and } \Gamma_2 = \Gamma_{S\varphi_2\varphi_2}^{\text{t-1}}(x = M) . \quad (6)$$

Then, the total on-shell tree-level decay width reads

$$\Gamma = \Gamma_S^{\text{t-1}}(x = M) = \Gamma_1 + \Gamma_2 . \quad (7)$$

As a consequence, the tree-level (or Breit-Wigner) expression of the survival probability  $p(t)$  for the resonance  $S$  created at  $t = 0$  is the usual exponential function

$$p_{\text{BW}}(t) = e^{-\Gamma t} , \quad (8)$$

and the corresponding tree-level expression of the mean lifetime is  $\tau_{\text{BW}} = 1/\Gamma$ . The explicit derivation of the exponential form is obtained through the Breit-Wigner limit in Sec. 2.3.

## 2.2 The mass distribution $d_S(x)$ and the survival probability $p(t)$

A crucial intermediate step toward the determination of the survival probability  $p(t)$  in the framework of quantum field theory is the evaluation of the propagator  $G_S(p^2)$  of the unstable resonance  $S$ . The quantity  $G_S(p^2)$  is obtained at the 1-loop level by (re)summing the one-particle irreducible self-energy contribution (Fig. 1, panel (b)):

$$G_S(p^2) = \left[ p^2 - M_0^2 + (\sqrt{2}g_1)^2 \Sigma(p^2, m_1^2) + (\sqrt{2}g_2)^2 \Sigma(p^2, m_2^2) + i\varepsilon \right]^{-1} , \quad (9)$$

where  $\Sigma(p^2, m^2)$  is the amplitude of the standard loop diagram in which two virtual particles of the  $\varphi$ -type circulate:

$$\Sigma(p^2, m^2) = -i \int \frac{d^4 q}{(2\pi)^4} \frac{1}{\left[ \left( \frac{p}{2} + q \right)^2 - m^2 + i\varepsilon \right] \left[ \left( \frac{p}{2} - q \right)^2 - m^2 + i\varepsilon \right]} . \quad (10)$$

---

<sup>1</sup>Alternatively, one could introduce a counterterm and work with  $M_0$  as the physical mass, see details in Appendix 1.

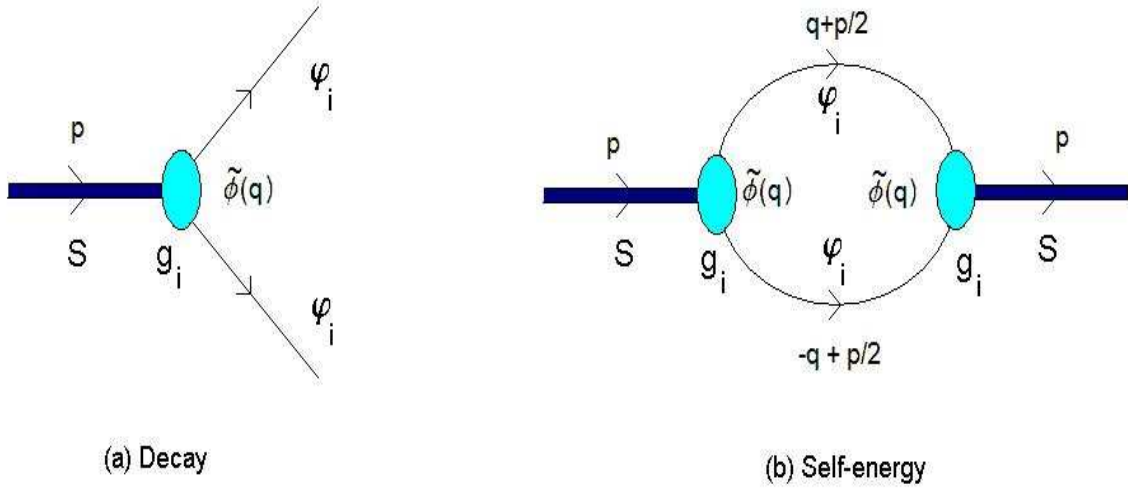


Figure 1: Pictorial representation of (a) the amplitude of the tree-level decay process  $S \rightarrow \varphi_i \varphi_i$  with  $i = 1, 2$  and (b) the corresponding self-energy diagram. The imaginary part of (b) is related to (a), see Eq. (13) and the discussion in the text. The quantity  $\tilde{\phi}(q)$  is the vertex function, which is chosen to be  $\tilde{\phi}(q) = \theta(\Lambda^2 - \mathbf{q}^2)$  for the numerical evaluations.

It is also useful for future purposes to introduce the function  $\Pi(p^2)$  as

$$\Pi(p^2) = (\sqrt{2}g_1)^2 \Sigma(p^2, m_1^2) + (\sqrt{2}g_2)^2 \Sigma(p^2, m_2^2), \quad (11)$$

in such a way that the propagator is given by the simple expression:

$$G_S(p^2) = [p^2 - M_0^2 + \Pi(p^2) + i\varepsilon]^{-1}. \quad (12)$$

Due to the optical theorem the imaginary part of the function  $\Pi(p^2 = x^2)$  is related to the tree-level decay function in Eq. (4):

$$\text{Im } \Pi(x^2) = x \Gamma_S^{t-1}(x). \quad (13)$$

Although the imaginary part is convergent, this is not the case for the real part. For this reason the loop function  $\Sigma(p^2, m^2)$  must be regularized: in this work we use a sharp, three-dimensional cutoff  $\Lambda$  for the explicit numerical examples. However, different choices of the regularization procedures do not change the qualitative features of the discussion [14, 15, 16]. The explicit expression for the function  $\Sigma(p^2, m^2)$  and more details on the consequences of the optical theorem are given in Appendix A.

The spectral function  $d_S(x)$  of the scalar field  $S$  is defined as the imaginary part of the propagator:

$$d_S(x = \sqrt{p^2}) = \frac{2x}{\pi} \left| \lim_{\varepsilon \rightarrow 0} \text{Im}[G_S(x^2)] \right|. \quad (14)$$

Explicitly:

$$d_S(x) = \frac{2x}{\pi} \lim_{\varepsilon \rightarrow 0} \frac{\text{Im}[\Pi(x^2)] + \varepsilon}{(x^2 - M_0^2 + \text{Re} \Pi(x^2))^2 + (\text{Im} \Pi(x^2) + \varepsilon)^2}. \quad (15)$$

The renormalized mass  $M$  of the particle  $S$  is defined as the zero of the real part of  $G_S(p^2)^{-1}$ :

$$M^2 - M_0^2 + \text{Re} \Pi(M^2) = 0. \quad (16)$$

Usually,  $\text{Re} \Pi(M^2) > 0$ , thus the renormalized mass  $M$  is smaller than  $M_0$ .

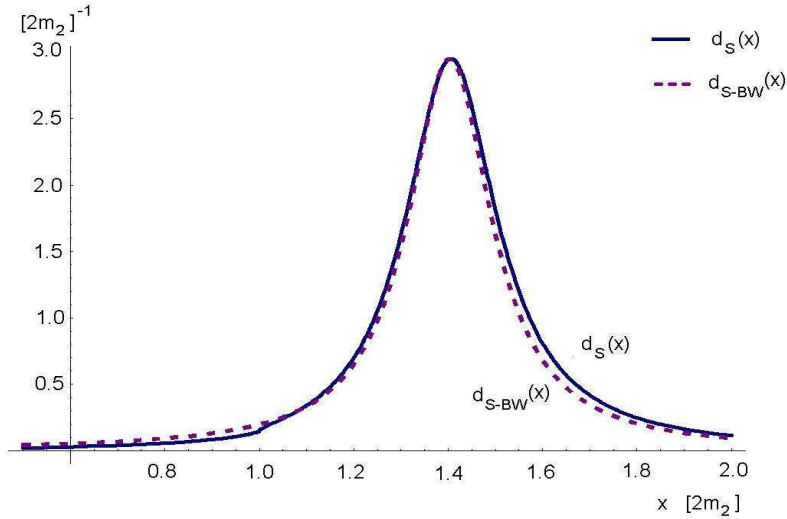


Figure 2: The spectral function  $d_S(x)$  from Eq. (14) and the nonrelativistic BW limit  $d_{S-BW}(x)$ , see Eq. (30) derived in Sec. 2.3, are plotted for the numerical values of Eq. (18). In this example the function  $d_S(x)$  differs only slightly from the BW limit, but this small deviation is enough to generate sizable deviations in the early temporal evolution, see later on.

The quantity  $d_S(x)dx$  represents the probability that in the rest frame of  $S$  the state  $S$  has a mass between  $x$  and  $x + dx$ . For this reason it is also denoted as the mass distribution of the unstable state  $S$ . It is correctly normalized for each  $g_1, g_2$ ,

$$\int_0^\infty dx d_S(x) = 1, \quad (17)$$

and, in the limit  $g_1 \rightarrow 0$  and  $g_2 \rightarrow 0$ , the expected spectral function  $d_S(x) = \delta(x - M_0)$  is obtained, see details in Refs. [16, 17].

In Fig. 2 we present the spectral function  $d_S(x)$  for a selected numerical example, where we chose as energy unit the quantity  $[2m_2]$ :

$$M_0 = \frac{3}{2} [2m_2], \quad g_1 = g_2 = 3 [2m_2], \quad m_1 = \frac{1}{10} [2m_2], \quad m_2 = \frac{1}{2} [2m_2], \quad \Lambda = 2 [2m_2]. \quad (18)$$

As a result one obtains from Eq. (16) that  $M = 1.40 [2m_2]$  (which is just slightly smaller than  $M_0$ : the quantum fluctuations are not large in this example). The tree-level decay widths read:  $\Gamma_1 = 0.13 [2m_2]$ ,  $\Gamma_2 = 0.089 [2m_2]$  and  $\Gamma = 0.22 [2m_2]$ . As a consequence, the tree-level lifetime reads  $\tau_{BW} = 4.63 [2m_2]^{-1}$ . We shall use these numerical values in all the upcoming plots of the paper, because they allow for a clear visualization of the underlying equations. It should be however stressed that the qualitative behavior is not dependent on the precise numerical choice.

It is now possible to determine the probability amplitude  $a(t)$ , and therefore the survival probability  $p(t)$ . To this end, let us consider the set  $\{|x\rangle\}$  of eigenstates of the full Hamiltonian  $H$  of the system defined by the Lagrangian of Eq. (1):  $H|x\rangle = x|x\rangle$ . The continuous variable  $x$  describes two-particle states and therefore is such that  $x \geq 2m_1$ . The survival amplitude  $a(t)$  reads (in the Heisenberg picture)

$$a(t) = \langle S | e^{-iHt} | S \rangle = \langle S | x \rangle e^{-ixt} \langle x | S \rangle = |\langle S | x \rangle|^2 e^{-ixt}, \quad (19)$$

where the integration over the continuous variable  $x$  is understood. Taking into account that  $|\langle S | x \rangle|^2 = d_S(x)$  (i.e., as shown above,  $d_S(x)dx$  is the probability that the unstable state  $S$  has an energy between  $x$  and  $x + dx$ ) and making the integration explicit, we get:

$$a(t) = \int_{-\infty}^{\infty} dx d_S(x) e^{-ixt}, \quad p(t) = |a(t)|^2. \quad (20)$$

The integrand in Eq. (20) is nonzero only between  $(2m_1, \infty)$  in virtue of the step function in Eq. (13). However, it is from a technical point of view helpful to write the integration range as  $(-\infty, \infty)$  so that the quantity  $a(t)$  is expressed as the Fourier transform of the spectral function  $d_S(x)$ . It is in this way that the usual exponential law can be derived in the so-called Breit-Wigner limit, see Sec. 2.3.

The condition  $p(0) = 1$  is fulfilled in virtue of the normalization of  $d_S(x)$ . This property is, in turn, a consequence of the resummation and of the validity of the so-called Källen-Lehman representation [17]. In Fig. 3 the function  $p(t)$  and the corresponding exponential limit  $p_{\text{BW}}(t) = e^{-\Gamma t}$  are plotted: it is evident that sizable deviations from the ‘full’ result  $p(t)$  take place<sup>2</sup>. This fact is remarkable if one considers that the deviations of the spectral function  $d_S(x)$  from the Breit-Wigner limit  $d_{S\text{-BW}}(x)$  are very small, see Fig. 2. Nevertheless, these small deviations are enough to generate large changes in the temporal evolution of the system: for a better visualization of this point, the difference  $p(t) - p_{\text{BW}}(t)$  has been also plotted in Fig. 3.

The spectral function  $d_S(x)$  is naturally bound from below because of the presence of the low-energy threshold  $2m_1$ . Its behavior for large energies  $x$  can be easily inferred by using the optical theorem in Eq. (13):  $d_S(x) \sim x^{-3}$  for large  $x$ . Then, the presence of cutoff  $\Lambda$  implies that  $d_S(x) = 0$  for  $x > 2\sqrt{\Lambda^2 + m_1^2} \approx 2\Lambda$ . It thus follows that the mean energy

$$\langle x \rangle = \int_{-\infty}^{\infty} dx x d_S(x) \quad (21)$$

is a finite number. As shown in Ref. [1] the existence of an energy threshold and the finiteness of  $\langle x \rangle$  suffice to guarantee short-time (and also and long-time) deviations from the exponential decay law. Quite remarkably, in the present superrenormalizable model of Eq. (1) the finiteness of  $\langle x \rangle$  is guaranteed also in the limit  $\Lambda \rightarrow \infty$ , being  $x d_S(x) \sim x^{-2}$  for large  $x$ . On the contrary, all higher momenta  $\langle x^n \rangle = \int_{-\infty}^{\infty} dx x^n d_S(x)$  with  $n = 2, 3, \dots$  diverge for  $\Lambda \rightarrow \infty$ . As shown in Ref. [18], the finiteness of  $\langle x \rangle$  also assures the differentiability of the amplitude  $a(t)$  (and thus also of  $p(t)$ ), which we will use in the following considerations and also in Secs. 2.4 and 2.5 when discussing in more detail the short-time behavior and the quantum-Zeno effect.

We now introduce the decay probability density  $h(t)$ : the quantity  $h(t)dt$  represents the probability that the unstable particle  $S$  decays in the time interval  $(t, t + dt)$ . Clearly, the integrated quantity  $w(t)$  defined as

$$w(t) = \int_0^t du h(u) = 1 - p(t) \quad (22)$$

represents the probability that the unstable particle decays between 0 and  $t$ . Deriving the latter equation we obtain

$$h(t) = -\frac{dp}{dt} = -p'(t), \quad (23)$$

i.e.  $h(t)$  is simply the negative derivative of the survival probability  $p(t)$ .

In terms of state vectors the probability  $w(t)$  can be symbolically expressed as

$$w(t) = \int_0^t du h(u) = \sum_{i=1,2} \sum_{\mathbf{k}} |\langle \varphi_{i,\mathbf{k}} \varphi_{i,-\mathbf{k}} | e^{-iHt} | S \rangle|^2, \quad (24)$$

where the state  $|\varphi_{i,\mathbf{k}} \varphi_{i,-\mathbf{k}}\rangle$  represents the state of two particles of the type  $\varphi_i$ , which carry opposite three-momentum  $\mathbf{k}$  and  $-\mathbf{k}$ , respectively. In fact, the object  $|\langle \varphi_{i,\mathbf{k}} \varphi_{i,-\mathbf{k}} | e^{-iHt} | S \rangle|^2$  is the probability that the particle  $S$  decays into two particles of the type  $\varphi_i$ , the first with momentum  $\mathbf{k}$  and the second

<sup>2</sup>Here ‘full’ result means that the resummed 1-loop approximation has been performed and that the full functional form of the spectral function  $d_S(x)$  is kept in the evaluation of the temporal behavior.

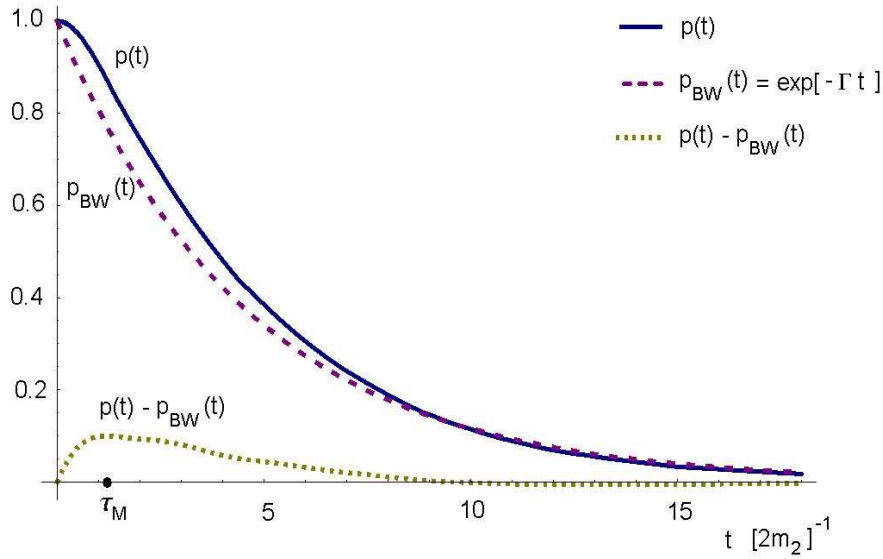


Figure 3: The survival probability  $p(t)$ , the BW limit  $p_{\text{BW}}(t) = e^{-\Gamma t}$  and the difference  $p(t) - p_{\text{BW}}(t)$  are plotted for the numerical values of Eq. (18). The dot on the horizontal axis corresponds to the value of  $\tau_M$ , see Eq. (40) and the discussion in Sec. 2.4.

with momentum  $-\mathbf{k}$ . The overall decay probability  $w(t)$  results as the sum of all these (independent) probabilities. It is important to stress that in Eq. (24) we neglect the decays into  $n$ -particle states with  $n = 4, 6, 8, \dots$ , which are suppressed by kinematical factors and anyhow neglected in the self-energy contributions. Note also that the summation  $\sum_{\mathbf{k}}$  means the sum over all the momenta  $\mathbf{k} = 2\pi\mathbf{n}/L$ , where  $\mathbf{n} = (n_1, n_2, n_3)$  and  $n_i = 0, \pm 1, \pm 2, \dots$ ; the system is thus confined into a box with volume  $V = L^3$ . The limit  $L \rightarrow \infty$  is straightforward but unnecessary for the present discussion (see Sec. 3.1 for the explicit evaluation of it).

Upon deriving Eq. (24) we can also express  $h(t)$  in terms of state vectors:

$$h(t) = \frac{d}{dt} \left( \sum_{i=1,2} \sum_{\mathbf{k}} |\langle \varphi_{i,\mathbf{k}} \varphi_{i,-\mathbf{k}} | e^{-iHt} | S \rangle|^2 \right). \quad (25)$$

It is indeed a remarkable fact that, in order to evaluate  $h(t)$  we do not need to evaluate explicitly the matrix elements  $\langle \varphi_{i,\mathbf{k}} \varphi_{i,-\mathbf{k}} | e^{-iHt} | S \rangle$ , but we simply have to perform the derivative of Eq. (23).

In Fig. 4 the density of decay probability  $h(t)$  and its corresponding BW limit  $h_{\text{BW}}(t) = -p'_{\text{BW}}(t) = \Gamma e^{-\Gamma t}$  are plotted. Here the difference between the ‘full’ result and the BW limit are even more evident, due to the fact that  $h(t \rightarrow 0)$  vanishes and  $h_{\text{BW}}(t \rightarrow 0) = \Gamma$  clearly does not, see Sec. 2.4 for a detailed description of this point. Moreover, one can clearly see the presence of oscillations of the function  $h(t)$ , in agreement with the discussion of Ref. [11].

### 2.3 The Breit-Wigner limit

It is instructive to discuss the Breit-Wigner limit, in which the survival probability  $p(t)$  turns out to be exponential. We start by approximating  $d_S(x)$  as follows:

$$d_S(x) = \frac{2x}{\pi} \frac{x\Gamma_S^{t-1}(x)}{(x^2 - M_0^2 + \text{Re}\Pi(x^2))^2 + (x\Gamma_S^{t-1}(x))^2} \simeq \frac{2M}{\pi} \frac{M\Gamma_S^{t-1}(M)\theta(x - 2m_1)}{(x^2 - M^2)^2 + (M\Gamma_S^{t-1}(M))^2}. \quad (26)$$

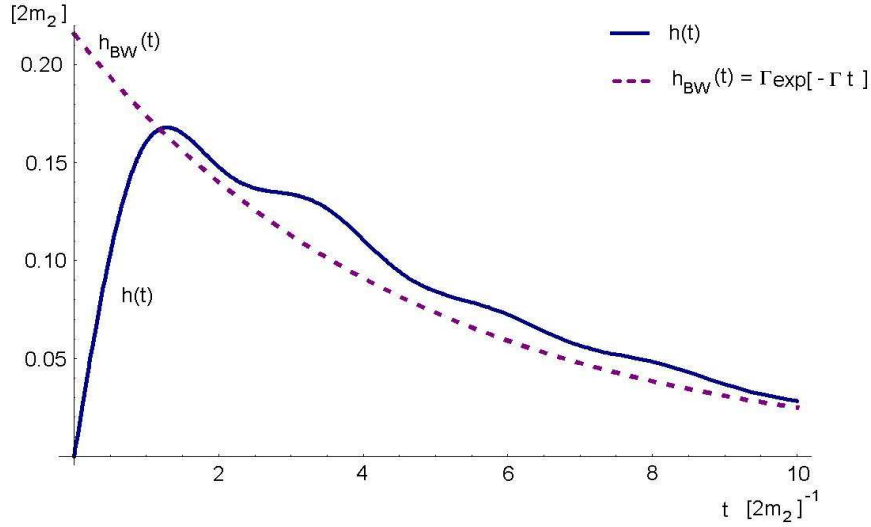


Figure 4: The decay probability density  $h(t)$  and the corresponding BW limit  $h_{\text{BW}}(t) = \Gamma e^{-\Gamma t}$  are plotted for the numerical choice of Eq. (18). For short times the two functions are qualitatively (and here also quantitatively) very different, while the former vanishes and the latter does not. Moreover, oscillations on top of the exponential are visible. Then, for large times the function  $h(t)$  approaches the BW limit  $h_{\text{BW}}(t)$ .

By having included the step function  $\theta(x - 2m_1)$  we have kept track of the threshold. A subtle point of Eq. (26) is the normalization, which is spoiled by the employed approximation. This property is however crucial in order to have  $p(0) = 1$ . It is thus necessary to rescale the function in such a way that it is normalized to 1. Finally, the spectral function in the relativistic BW approximation reads:

$$d_{S\text{-BWrel}}(x) = \frac{N_{\text{BWrel}}}{(x^2 - M^2)^2 + (M\Gamma)^2} \theta(x - 2m_1), \quad (27)$$

where

$$N_{\text{BWrel}} = \left[ \int_{-\infty}^{\infty} dx \frac{\theta(x - 2m_1)}{(x^2 - M^2)^2 + (M\Gamma)^2} \right]^{-1} = \left[ \int_{2m_1}^{\infty} dx \frac{1}{(x^2 - M^2)^2 + (M\Gamma)^2} \right]^{-1}. \quad (28)$$

A further simplification, leading to the usual, nonrelativistic Breit-Wigner form, is needed:

$$\begin{aligned} d_{S\text{-BWrel}}(x) &= \frac{N_{\text{BWrel}} \theta(x - 2m_1)}{(x^2 - M^2)^2 + (M\Gamma)^2} = \frac{N_{\text{BWrel}} \theta(x - 2m_1)}{(x - M)^2 (x + M)^2 + (M\Gamma)^2} \\ &\simeq \frac{N_{\text{BWrel}} \theta(x - 2m_1)}{(x - M)^2 (2M)^2 + (M\Gamma)^2} \simeq \frac{N_{\text{BWrel}}}{(x - M)^2 (2M)^2 + (M\Gamma)^2}. \end{aligned} \quad (29)$$

Note that in the last equation we have also dropped the requirement that  $x > 2m_1$ , thus  $x$  can now vary from  $-\infty$  to  $+\infty$ . This is of course unphysical for the present Hamiltonian because negative values of  $x$ , i.e. negative values of the running mass of the unstable state  $S$ , do not make sense. Nevertheless, the function is peaked at  $M > 0$  and the extension to negative  $x$  affects the function for  $x > 2m_1$  only negligibly<sup>3</sup>. As a result, the spectral function in the nonrelativistic BW approximation reads

$$d_{S\text{-BW}}(x) = \frac{N_{\text{BW}}}{(x - M)^2 + \Gamma^2/4}, \quad (30)$$

<sup>3</sup>This is true for the nonrelativistic approximation, but is not true for the relativistic one: in fact, the latter is peaked also for  $x = -M$ .

where  $N_{\text{BW}} = \Gamma/2\pi$  is the normalization constant such that  $\int_{-\infty}^{\infty} dx d_{S\text{-BW}}(x) = 1$ .

The amplitude  $a(t)$  as calculated from Eqs. (20) and (30) takes the form

$$a_{\text{BW}}(t) = e^{-\Gamma t/2} e^{-iMt} \quad (t > 0) \quad (31)$$

which implies the exponential decay law

$$p_{\text{BW}}(t) = |a_{\text{BW}}(t)|^2 = e^{-\Gamma t} . \quad (32)$$

Notice that this result has been obtained by extending the range of integration in Eq. (20) to  $(-\infty, \infty)$ . Obviously, the Breit-Wigner distribution is never exact and cannot be fulfilled by any physical system. It is in this sense remarkable that deviations from the exponential decay law have been discussed only relatively recently. This has surely to do with the fact that the BW distribution, although never exact, works extremely well for the majority of physical systems in a sufficiently large energy interval. Conversely, as function of time the deviations from the exponential law take place very early and very late, and are thus difficult to measure.

The decay probability density  $h(t)$  defined in Eq. (23) shows also an exponential behavior in the BW limit:

$$h(t) \rightarrow h_{\text{BW}}(t) = -p'_{\text{BW}}(t) = \Gamma e^{-\Gamma t} . \quad (33)$$

The exponential functions  $p_{\text{BW}}(t)$  and  $h_{\text{BW}}(t)$  have been plotted and compared with the ‘full’ results  $p(t)$  and  $h(t)$  in Fig. 3 and 4, respectively.

## 2.4 Vanishing of $p'(0)$ and the definition of the ‘Zeno-time’

Let us consider the first derivative of the survival probability  $p(t)$  for  $t = 0$ ,  $p'(0)$ . To this end we study the quantity

$$a'(t) = \int_{-\infty}^{\infty} dx (-ix) d_S(x) e^{-ixt} . \quad (34)$$

In virtue of the cutoff (independently on its value) the integral  $\int_{-\infty}^{\infty} dx x d_S(x) e^{-ixt}$  is well defined and does not contain any divergences. In particular

$$a'(t=0) = -i \int_{-\infty}^{\infty} dx x d_S(x) = -i \langle x \rangle \quad (35)$$

is a well defined imaginary number, being  $\langle x \rangle$  a finite real number, as discussed in Sec. 2.2.

The function  $p'(t)$  can be expressed as

$$p'(t) = a'^*(t) a(t) + a^*(t) a'(t) . \quad (36)$$

Being  $a(0) = 1$  we obtain

$$p'(0) = i \langle x \rangle - i \langle x \rangle = 0. \quad (37)$$

The first derivative of the survival probability vanishes for  $t = 0$ . This means that for small times a deviation from the exponential law, for which one obviously has  $\lim_{t \rightarrow 0^+} p'_{\text{BW}}(t) = -\Gamma$  (see Eq. (32)), is realized.

The natural question is how long does the deviation from the exponential law lasts. In the literature a Taylor expansion has been often performed,

$$p(t) = 1 - \frac{t^2}{\tau_Z^2} + \dots , \quad (38)$$

where the coefficient

$$\tau_Z = \sqrt{\frac{1}{\langle x^2 \rangle - \langle x \rangle^2}} \quad (39)$$

has been defined as the ‘Zeno time’, which quantifies the time interval of non-exponential behavior. However, as already explained in Ref. [14], the second order derivative does not even need to exist. As a trivial illustrative example one can consider the simple and well defined function  $p(t) = 1 - t^{3/2}$ , for which  $p'(0) = 0$  but  $p^{(n>1)}(0) = \infty$ . Moreover, even when the second derivative exists –as in all physical cases, see below– this does not necessarily mean that the parameter  $\tau_Z$  in Eq. (38) represents a correct estimate of the time interval in which a deviation from the exponential law takes place.

In order to overcome this problem, in Ref. [14] a definition has been introduced which does not depend on the Taylor expansion of the function  $p(t)$ . The time  $\tau_M$  is defined as the instant of time at which the deviation of the function  $p(t)$  from the exponential behavior  $e^{-\Gamma t}$  is maximal:

$$\max (p(t) - e^{-\Gamma t}) \rightarrow t = \tau_M . \quad (40)$$

Clearly

$$\frac{d}{dt} (p(t) - e^{-\Gamma t})_{t=\tau_M} = 0 ; \quad (41)$$

in all practical cases  $\tau_M$  corresponds to the first zero of the derivative of the function  $p(t) - e^{-\Gamma t}$ . The function  $p(t) - e^{-\Gamma t}$  has been plotted in Fig. 3 for the numerical values of Eq. (18). The maximum is realized for  $\tau_M = 1.18 [2m_2]^{-1}$ , implying the ratio  $\tau_M/\tau_{BW} = 0.26$ . In the present model, the non-exponential behavior elapses for  $\sim 2\tau_M$ , meaning that in this example is about 50% of the tree-level lifetime of the unstable particle.

Further comments are in order:

(i) In the present work we consider field theoretical examples with some finite value of the cutoff. It is indeed a natural requirement that at some energy  $x \gtrsim \Lambda$  the loop function  $\Sigma(x^2, m^2)$  is suppressed. The actual value of the constant  $\Lambda$  depends on the theory under study. For instance, working with hadronic theories implies  $\Lambda \sim 1\text{-}2 \text{ GeV}$  [19]. On the contrary, for elementary Standard Model processes, the cutoff  $\Lambda$  is of the order of  $M_{\text{Planck}}$  (alternatives are  $\Lambda \sim M_{GUT} \sim 10^{16} \text{ GeV}$  and, in some recent scenarios with large extradimension(s), even smaller with  $\Lambda \gtrsim 1 \text{ TeV}$ ).

(ii) One can also regard the theory of Eq. (1) as a (super)renormalizable toy model with a very large value of the cutoff, such as  $\Lambda \sim M_{\text{Planck}} \sim 10^{19} \text{ GeV}$ . In this case the first derivative vanishes,  $p'(0) = 0$ , and all the other derivatives, including the second derivative  $p''(0)$ , are large but finite: for instance, the quantity  $p''(0)$  is proportional to  $\ln \Lambda$ . This is easily understandable, being the asymptotic behavior for large  $x$  given by  $d_S(x) \sim x^{-3}$ , thus implying that  $\langle x^2 \rangle = \int_{-\infty}^{\infty} x^2 d_S(x) dx \sim \ln \Lambda$ . In the present superrenormalizable case, the functions  $p(t)$  for  $\Lambda \sim 1\text{-}2 \text{ GeV}$  and for  $\Lambda \sim M_{\text{Planck}}$  differ only slightly: the deviations from the exponential law last for a similar amount of time and the value of the ratio  $\tau_M/\tau_{BW}$  shows a very weak dependence on the cutoff [14]. This example shows that, in the case of large  $\Lambda$  (as for instance,  $\Lambda \sim M_{\text{Planck}}$ ), although the Zeno time  $\tau_Z \sim 1/\sqrt{\ln \Lambda}$  turns out to be very small (as it was obtained in Refs. [20, 21] in the framework of perturbation theory),  $\tau_Z$  offers only an underestimation of the actual non-exponential time interval, which is sizable also for large values of the cutoff.

(iii) In the nonrelativistic Breit-Wigner limit of Eq. (30) the first derivative  $p'(0)$  is –strictly speaking– not defined. However, by using the fact that the amplitude reads  $p_{BW}(t > 0) = e^{-\Gamma t}$ , one obviously has  $\lim_{t \rightarrow 0^+} p'_{BW}(t) = -\Gamma$ . In other words, the function  $p'_{BW}(t)$  can be easily continued to the point  $t = 0$ .

(iv) The present results are based on the (resummed) 1-loop approximation. The inclusion of higher order, such as the sunset diagram in which a particle  $S$  is exchanged by the two particles  $\varphi$  circulating in the loop of Fig. 1.b, is a task for the future. It is expected that higher order terms do not change substantially the results: in fact, higher order diagrams are suppressed by the multiplication of vertex functions. (Moreover, in the framework of hadronic theories, higher order are suppressed in the so-called large- $N_c$  approximation [22]. The behavior of a theory similar to that of Eq. (1) in the large- $N_c$  limit is discussed in Ref. [23]).

(v) The resummation of the loop diagram in Fig. 1.b, expressed in its unregularized form in Eq. (10) and in its regularized form in Eq. (144) reported in the Appendix A, has been a crucial

step toward the presented results, also in connection with the correct normalization of  $p(t)$  and the vanishing of  $p'(0)$  (necessary to show the non-exponential behavior). If, instead, one would consider only the perturbative expressions of the propagator at the 1-loop ( $g_i^2$ ) level, one obtains

$$G_S^{\text{pert}}(p^2) = \frac{1}{p^2 - M_0^2 + i\varepsilon} + \left( \frac{1}{p^2 - M_0^2 + i\varepsilon} \right)^2 \left[ (\sqrt{2}g_1)^2 \Sigma(p^2, m_1^2) + (\sqrt{2}g_2)^2 \Sigma(p^2, m_2^2) \right] + \dots, \quad (42)$$

thus the spectral function in this case would take the form

$$d_S^{\text{pert}}(x) = \frac{2x}{\pi} \text{Im} G_S^{\text{pert}}(p^2 = x^2) = \delta(x - M_0) + \frac{4g_1^2}{\pi} \frac{\sqrt{\frac{x^2}{4} - m_1^2}}{(x^2 - M_0^2)^2} + \frac{4g_2^2}{\pi} \frac{\sqrt{\frac{x^2}{4} - m_2^2}}{(x^2 - M_0^2)^2} + \dots \quad (43)$$

The normalization of  $d_S^{\text{pert}}(x)$  is not anymore explicitly fulfilled for each value of  $g$  and an unphysical singularity for the bare value of the mass  $x = M_0$  is present. (This infinity is removed when the resummation is performed.) It would be cumbersome to derive analytical results with this perturbative expressions; moreover, a numerical study could hardly be performed, thus showing the necessity of the resummation *before* the temporal analysis is investigated.

(vi) The issue of the preparation of the state  $|S\rangle$  at the time  $t = 0$  is well defined when the state is long lived, but more controversial for short living particles. A related difficulty is the (in)dependence on the representation choice [24], see also the corresponding discussions in Ref. [14]. Here it suffices to say that the change of the representation of the fields is equivalent to the change of the initial state. Nevertheless, also in this case deviations from the exponential law take place, but the mass distribution would have a different form.

(vii) As a last step we discuss the validity of the employed model of Eq. (1) upon variation of the parameters. The choice of the numerical values in Eq. (18) has been done in order to obtain figures which allow for a clear presentation of the underlying equations. However, the described patterns take place also when the parameters are varied: in particular, when the coupling constants  $g_1$  and  $g_2$  are decreased, the time interval in which sizable variations from the exponential decay law take place becomes smaller. In the opposite direction, when the coupling constants  $g_1$  and  $g_2$  become larger, this time interval grows. However, care is needed when increasing the values of the coupling constants: beyond a certain threshold, the validity of the Källén-Lehman representation, and thus of the normalization condition of Eq. (17), does not any longer hold, see the detailed discussion in Ref. [17]. Note also that the QFT model of Eq. (1) does not show, for any value of the parameters, repopulation effect. In fact, the function  $h(t)$  is always positive in this model.

## 2.5 The quantum Zeno effect

It is interesting and amusing to briefly review the so-called quantum Zeno effect. To this end we define the function  $\gamma(t)$  as in Ref. [4]:

$$\gamma(t) = -\frac{\ln p(t)}{t} \leftrightarrow p(t) = e^{-\gamma(t)t}. \quad (44)$$

In Fig. 5 the function  $\gamma(t)$  is plotted and is compared to the tree-level decay width  $\Gamma$ . It is visible that for short times  $\gamma(t)$  is considerably smaller than  $\Gamma$ , see the discussion below.

Let us now suppose to perform a single measurement of the system at the time  $\tau > 0$ . The probability that the unstable state  $S$  did not decay at the time  $\tau$  reads

$$p_\tau = p(\tau) = e^{-\gamma(\tau)\tau} \simeq e^{-\Gamma\tau} \quad (45)$$

where in the last passage we assumed that the time  $\tau$  is large enough in order that  $\gamma(\tau) \simeq \Gamma$ .

Instead, let us suppose to perform  $N$  measurements at the time intervals  $t_*$ , such that  $\tau = Nt_*$ . The probability that at the time  $\tau$  (after the  $N$  measurements) the state did not decay is given by

$$p_{N-t_*} = \left( e^{-\gamma(t_*)t_*} \right)^N = e^{-\gamma(t_*)Nt_*} = e^{-\gamma(t_*)\tau}. \quad (46)$$

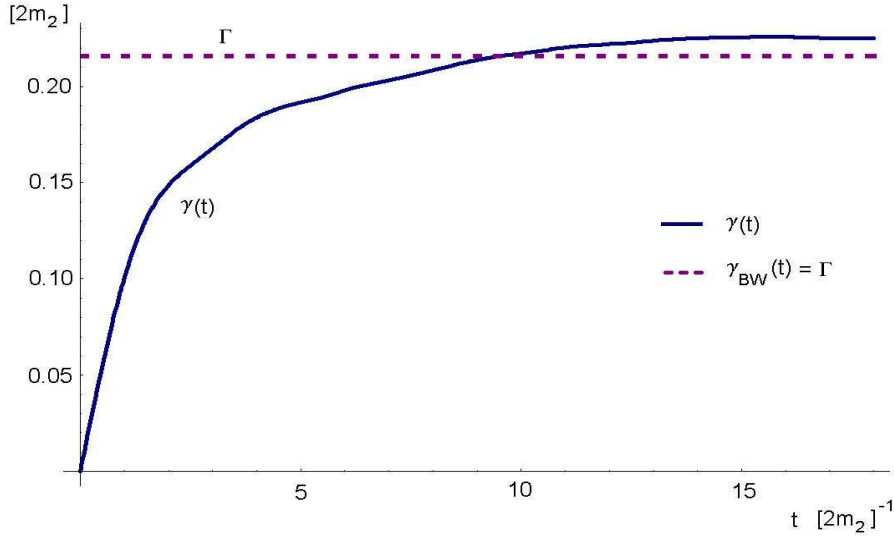


Figure 5: The function  $\gamma(t) = -[\ln p(t)]/t$  is plotted. For comparison, the constant BW limit  $\gamma_{\text{BW}}(t) = -[\ln p_{\text{BW}}(t)]/t = \Gamma$  is also shown. For short times  $\gamma(t) < \Gamma$ , rendering the quantum Zeno effect possible. As usual, the numerical values of Eq. (18) have been used.

When  $t_*$  belongs to the ‘non-exponential’ time-interval,  $0 \leq t_* \lesssim \tau_M$ , one has  $\gamma(t_*) < \Gamma$ . Indeed, considering that the function  $\gamma(t)$  vanishes for  $t = 0$ ,

$$\gamma(0) = \left( -\frac{p'(t)}{p(t)} \right)_{t=0} = -p'(0) = 0, \quad (47)$$

one can make the quantity  $\gamma(t_*)$  as small as desired by choosing  $t_* \ll \tau_M$ .

In general, for  $0 \leq t_* \lesssim 2\tau_M$ , the inequality

$$p_{N-t_*} = e^{-\gamma(t_*)\tau} > p_\tau \simeq e^{-\Gamma\tau}. \quad (48)$$

holds. Its meaning is clear but astonishing: the subsequent measurements of the unstable particle  $S$  increased the probability that it did not decay. (Formally, one performs a ‘measurement’ of the unperturbed Hamiltonian  $H_0$ , in which the coupling constants  $g_i$  are set to zero). This property has been indeed verified experimentally by using ions trapped in a potential barrier [9].

For  $t_* \rightarrow 0$ , i.e. for  $N \rightarrow \infty$  (a situation which corresponds to a ‘continuous’ measurement) one obtains that  $p_{N-t_*} \rightarrow 1$ . The unstable particle does not decay at all! This is the famous quantum Zeno paradox.

As Fig. 5 shows, there are also time intervals in which  $\gamma(t) > \Gamma$ . This implies that for  $t_*$  satisfying this relation a faster decay rate is obtained when the state of the unstable particle is observed at intervals of  $t_*$ . This situation corresponds to the so called quantum Anti-Zeno effect [3, 4].

We conclude this brief recall of the Zeno effect by noticing that it does not take place in the Breit-Wigner limit. In fact, in this limit one has  $\gamma(t) = \Gamma$  for each  $t$ , thus meaning that  $p_{N-t_*} = p_\tau$ , independently on the value of  $t_*$  and  $\tau$ . Making a single measurements or many intermediate measurements does not lead to any change in the survival probability.

### 3 General properties of decays in QM: Lee Hamiltonian and link to QFT

#### 3.1 QM with Lee Hamiltonian(s)

We now study a similar system in the framework of quantum mechanics. In order to obtain irreversible dynamics in a QM approach, one needs to couple the unstable state  $|S\rangle$  to a continuum of states. The formalism described here relies on the so-called Lee Hamiltonians [12] (later on denoted also as QM-LH approach) and is a generalization to the two-channel case of the work in Ref. [4]. In this section we recall general properties of the LH approach with the special aim of showing the similarities with the genuine QFT approach presented in the previous section. In this context we also refer to Ref. [13], where a solvable Lee Hamiltonian has been studied in great detail and the relation to QFT has been described.

For transparency, we first present the Hamiltonian using a discrete sum and later on perform the transition to the continuous results. The Hamiltonian under consideration is given by

$$H = H_0 + H_{int} , H_{int} = H_{int}^{(1)} + H_{int}^{(2)} , \quad (49)$$

where

$$H_0 = M_0 |S\rangle \langle S| + \sum_{\mathbf{k}} \omega_1(\mathbf{k}) |1, \mathbf{k}\rangle \langle 1, \mathbf{k}| + \sum_{\mathbf{k}} \omega_2(\mathbf{k}) |2, \mathbf{k}\rangle \langle 2, \mathbf{k}| , \quad (50)$$

$$H_{int}^{(1)} = \sum_{\mathbf{k}} g_1 \frac{f_1(\mathbf{k})}{\sqrt{V}} (|1, \mathbf{k}\rangle \langle S| + |S\rangle \langle 1, \mathbf{k}|) , \quad (51)$$

$$H_{int}^{(2)} = \sum_{\mathbf{k}} g_2 \frac{f_2(\mathbf{k})}{\sqrt{V}} (|2, \mathbf{k}\rangle \langle S| + |S\rangle \langle 2, \mathbf{k}|) . \quad (52)$$

In order to establish a contact with the study of Sec. 2, the variable  $\mathbf{k}$  stays for  $\mathbf{k} = 2\pi\mathbf{n}/L$  and  $V = L^3$ . The analogy is clear: the state  $|S\rangle$  corresponds to the particle  $S$  of Eq. (1) and the states  $|1, \mathbf{k}\rangle, |2, \mathbf{k}\rangle$  are analogous to the two-particles states  $|\varphi_{1,\mathbf{k}}\varphi_{1,-\mathbf{k}}\rangle$  and  $|\varphi_{2,\mathbf{k}}\varphi_{2,-\mathbf{k}}\rangle$  of Sec. 2. The mixing terms in Eqs. (51)-(52) correspond to the interaction terms  $g_1 S\varphi_1^2$  and  $g_2 S\varphi_2^2$  of Eq. (1), respectively.

The transition to the continuous limit is obtained for

$$\sum_{\mathbf{k}} \rightarrow V \int \frac{d^3k}{(2\pi)^3} , |i, \mathbf{k}\rangle \rightarrow \sqrt{\frac{(2\pi)^3}{V}} |i, \mathbf{k}\rangle , i = 1, 2. \quad (53)$$

The time-evolution operator is given  $U(t) = e^{-iHt}$  can be expressed in terms of a Fourier transform:

$$U(t) = e^{-iHt} = \frac{i}{2\pi} \int_{-\infty}^{+\infty} dE \frac{1}{E - H + i\varepsilon} e^{-iEt} = \frac{i}{2\pi} \int_{-\infty}^{+\infty} dEG(E) e^{-iEt} , \quad (54)$$

where the operator

$$G(E) = \frac{1}{E - H + i\varepsilon} \quad (55)$$

has been introduced. One can rewrite  $G(E)$  as follow:

$$G(E) = \frac{1}{E - H + i\varepsilon} = \frac{1}{E - H_0 + i\varepsilon} \frac{1}{1 - \frac{H_{int}}{E - H_0 + i\varepsilon}} = \frac{1}{E - H_0 + i\varepsilon} \sum_{n=0}^{\infty} \left( H_{int} \frac{1}{E - H_0 + i\varepsilon} \right)^n \quad (56)$$

The propagator  $G_S(E)$  of the unstable state  $|S\rangle$  is defined as

$$G_S(E) = \langle S| G(E) |S\rangle \quad (57)$$

and can be evaluated using Eq. (56):

$$G_S(E) = \frac{1}{E - M_0 + i\varepsilon} \sum_{n=0}^{\infty} \langle S | \left( H_{int} \frac{1}{E - H_0 + i\varepsilon} \right)^n | S \rangle \quad (58)$$

Explicitly, the cases  $n = 1$  and  $n = 2$  read:

$$n = 1 \rightarrow \frac{1}{E - M_0 + i\varepsilon} \langle S | H_{int} | S \rangle = 0 , \quad (59)$$

$$n = 2 \rightarrow \langle S | \left( H_{int} \frac{1}{E - H_0 + i\varepsilon} \right)^2 | S \rangle = \langle S | H_{int} \frac{1}{E - H_0 + i\varepsilon} H_{int} | S \rangle \frac{1}{E - M_0 + i\varepsilon} . \quad (60)$$

The recursive quantity found for each  $n$  even is  $\Pi(E)$ :

$$\Pi(E) = - \langle S | H_{int} \frac{1}{E - H_0 + i\varepsilon} H_{int} | S \rangle = \quad (61)$$

$$- \langle S | H_{int} (|1, \mathbf{k}\rangle \langle 1, \mathbf{k}| + |2, \mathbf{k}\rangle \langle 2, \mathbf{k}|) \frac{1}{E - H_0 + i\varepsilon} (|1, \mathbf{q}\rangle \langle 1, \mathbf{q}| + |2, \mathbf{q}\rangle \langle 2, \mathbf{q}|) H_{int} | S \rangle , \quad (62)$$

where the sums over  $\mathbf{k}$  and  $\mathbf{q}$  are understood. Using Eqs. (51)-(52) and the orthonormality of the basis we get:

$$\Pi(E) = - \sum_{\mathbf{k}} \frac{1}{V} \frac{g_1^2 f_1^2(\mathbf{k})}{E - \omega_1(\mathbf{k}) + i\varepsilon} - \sum_{\mathbf{k}} \frac{1}{V} \frac{g_2^2 f_2^2(\mathbf{k})}{E - \omega_2(\mathbf{k}) + i\varepsilon} . \quad (63)$$

In the continuous limit the basic quantity  $\Pi(E)$  becomes:

$$\Pi(E) = - \int \frac{d^3 k}{(2\pi)^3} \frac{g_1^2 f_1^2(\mathbf{k})}{E - \omega_1(\mathbf{k}) + i\varepsilon} - \int \frac{d^3 k}{(2\pi)^3} \frac{g_2^2 f_2^2(\mathbf{k})}{E - \omega_2(\mathbf{k}) + i\varepsilon} = g_1^2 \Sigma_1(E) + g_2^2 \Sigma_2(E) . \quad (64)$$

The propagator  $G_S(E)$  of the state  $|S\rangle$  reads then

$$G_S(E) = \langle S | G(E) | S \rangle = \frac{1}{E - M_0 + \Pi(E) + i\varepsilon} . \quad (65)$$

The similarities between the present QM-LH approach and the QFT approach described in the previous section are clear (see for instance the form of the propagator in Eq. (9)), the main difference being the emergence of nonrelativistic propagator in the present case. The quantity  $\Pi(E)$  represents the analogous of the loop contributions.

We can now calculate the survival amplitude  $a(t) = \langle S | U(t) | S \rangle$ :

$$a(t) = \langle S | U(t) | S \rangle = \langle S | \frac{i}{2\pi} \int_{-\infty}^{+\infty} dE \frac{1}{E - H + i\varepsilon} e^{-iEt} | S \rangle = \frac{i}{2\pi} \int_{-\infty}^{+\infty} dE G_S(E) e^{-iEt} . \quad (66)$$

Using the dispersion relation

$$G_S(E) = \frac{1}{\pi} \int_{-\infty}^{\infty} dx \frac{\text{Im}[G_S(x)]}{x - E - i\varepsilon} \quad (67)$$

the survival amplitude  $a(t)$  can be expressed as

$$a(t) = \int_{-\infty}^{\infty} dx d_S(x) e^{-ixt} \quad (68)$$

where in this context the identification

$$d_S(x) = \frac{1}{\pi} |\text{Im}[G_S(x)]| \quad (69)$$

has been made. Again, the expression (69) and its QFT-counterpart of Eq. (14) are formally equivalent (a part from unimportant normalizations). Obviously, all the discussion about the deviations from the exponential law, the Breit-Wigner limit, the vanishing of  $p'(0)$  and the quantum Zeno effect can be easily repeated in the present QM-LH context.

### 3.2 Relativistic generalization of the LH and link to QFT

In order to obtain expressions which are equal to those of QFT of Sec. 2, one has to consider a slight modification of the Lee model. The issue is that in QFT one has particles with positive energy propagating forward in time and particles with negative energy propagating backwards in time (i.e. antiparticles). In our QFT model of Eq. (1) particles and antiparticles coincide, but it is anyhow the combination of both contributions which give rise to the usual relativistic propagator of the form  $1/(p^2 - m^2 + i\varepsilon)$ .

The QFT expressions can be obtained in a LH approach by modifying the time evolution operator (54) in the following way:

$$U(t) = \frac{i}{2\pi} \int_{-\infty}^{+\infty} dE \left( \frac{1}{E - H + i\varepsilon} + \frac{1}{E + H - i\varepsilon} \right) e^{-iEt} \quad (70)$$

$$= \frac{i}{2\pi} \int_{-\infty}^{+\infty} dE \frac{2E}{E^2 - H^2 + i\varepsilon} e^{-iEt} = \frac{i}{2\pi} \int_{-\infty}^{+\infty} dE 2EG(E) e^{-iEt}, \quad (71)$$

where the operator  $G(E)$  reads now

$$G(E) = \frac{1}{E^2 - H^2 + i\varepsilon}. \quad (72)$$

The integral has been done according to the famous Feynman prescription. If, as a simple example, one considers a free particle  $|S\rangle$  for which  $H_0^2 = M_0^2 |S\rangle \langle S|$ , one finds the usual propagator form (in the rest frame of  $S$ )  $G_S(E) = \langle S| G(E) |S\rangle = 1/(E^2 - M_0^2 + i\varepsilon)$ .

We consider a model in which we can write  $H^2$  as

$$H^2 = H_0^2 + H_{int}^2, \quad H_{int}^2 = H_{int}^{(1)2} + H_{int}^{(2)2} \quad (73)$$

where

$$H_0^2 = M_0^2 |S\rangle \langle S| + \sum_{\mathbf{k}} \omega_1^2(\mathbf{k}) |1, \mathbf{k}\rangle \langle 1, \mathbf{k}| + \sum_{\mathbf{k}} \omega_2^2(\mathbf{k}) |2, \mathbf{k}\rangle \langle 2, \mathbf{k}|, \quad (74)$$

$$H_{int}^{(1)2} = \sum_{\mathbf{k}} g_1 \frac{f_1(\mathbf{k})}{\sqrt{V}} (|1, \mathbf{k}\rangle \langle S| + |S\rangle \langle 1, \mathbf{k}|), \quad (75)$$

$$H_{int}^{(2)2} = \sum_{\mathbf{k}} g_2 \frac{f_2(\mathbf{k})}{\sqrt{V}} (|2, \mathbf{k}\rangle \langle S| + |S\rangle \langle 2, \mathbf{k}|). \quad (76)$$

We then follow the same steps of Sec. 3.1 and introduce the propagator as

$$G_S(E) = \langle S| G(E) |S\rangle = \frac{1}{E^2 - M_0^2 + \Pi(E) + i\varepsilon}, \quad (77)$$

where  $\Pi(E)$  is calculated in the same way as in Sec. 3.1 and –as expected– turns out to be the relativistic generalization of Eq. (64):

$$\Pi(E) = - \int \frac{d^3k}{(2\pi)^3} \frac{g_1^2 f_1^2(\mathbf{k})}{E^2 - \omega_1^2(\mathbf{k}) + i\varepsilon} - \int \frac{d^3k}{(2\pi)^3} \frac{g_2^2 f_2^2(\mathbf{k})}{E^2 - \omega_2^2(\mathbf{k}) + i\varepsilon} = g_1^2 \Sigma_1(E) + g_2^2 \Sigma_2(E). \quad (78)$$

Notice that the propagator  $G_S(E) = \langle S| G(E) |S\rangle$  takes a form which is formally equivalent to Eq. (9) obtained in QFT.

In particular, when we make the identifications

$$\omega_1^2(\mathbf{k}) = 4(\mathbf{k}^2 + m_1^2), \quad \omega_2^2(\mathbf{k}) = 4(\mathbf{k}^2 + m_2^2), \quad (79)$$

and

$$f_1(\mathbf{k}) = \sqrt{2} \frac{\tilde{\phi}(\mathbf{k})}{(\mathbf{k}^2 + m_1^2)^{1/4}}, \quad f_2(\mathbf{k}) = \sqrt{2} \frac{\tilde{\phi}(\mathbf{k})}{(\mathbf{k}^2 + m_2^2)^{1/4}}, \quad (80)$$

we get indeed in the present Lee model the *same* mathematical expression for the propagator of the QFT approach of Sec. 2. Note, the additional factor  $\sqrt{2}$  is here necessary to make contact with the identical particles in QFT and the cutoff function  $\tilde{\phi}(\mathbf{q})$  is described in detail in Appendix A and takes the form  $\tilde{\phi}(\mathbf{q}) = \theta(\Lambda^2 - \mathbf{q}^2)$  for the numerical evaluations presented in Figs. 2-10. Loosely speaking, the QFT case corresponds to a particular choice of the functions  $\omega_i(\mathbf{k})$  and  $f_i(\mathbf{k})$  of the Lee Hamiltonian studied here. This is an interesting property which we will use in Sec. 5.

By making use of dispersion relations we arrive at the usual expression for the survival amplitude  $a(t)$ :

$$a(t) = \int_{-\infty}^{\infty} dx d_S(x) e^{-ixt}, \quad (81)$$

where

$$d_S(x) = \frac{2x}{\pi} \left| \lim_{\varepsilon \rightarrow 0} \text{Im}[\langle S | G_S(x) | S \rangle] \right| \quad (82)$$

is identical to Eq. (14). This shows once more the tight connection of the present formalism with that of Sec. 2.

## 4 Two-channel case: quantum field theory

### 4.1 The decay probabilities $w_1(t)$ and $w_2(t)$ and the corresponding densities $h_1(t)$ and $h_2(t)$ : the formal expressions

In this section we come back to the quantum field theoretical model of Eq. (1). The central quantities under investigation are the decay probability densities  $h_1(t)$  and  $h_2(t)$  and the corresponding integrated decay probabilities  $w_1(t)$  and  $w_2(t)$ . The object  $h_1(t)dt$  represents the probability that the particle  $S$  decays in the first channel ( $S \rightarrow \varphi_1\varphi_1$ ) in the time interval between  $t$  and  $t + dt$ ; as a consequence, the integral  $w_1(t) = \int_0^t du h_1(u)$  represents the probability that the particle  $S$  decays into the first channel in the time interval  $(0, t)$ . The quantity  $w_1(t)$  can be formally expressed as the sum of the probabilities of decays into  $\varphi_1\varphi_1$  for different values of the three-momentum  $\mathbf{k}$ :

$$w_1(t) = \int_0^t du h_1(u) = \sum_{\mathbf{k}} |\langle \varphi_{1,\mathbf{k}}\varphi_{1,-\mathbf{k}} | e^{-iHt} | S \rangle|^2. \quad (83)$$

Similarly,  $h_2(t)dt$  represents the probability that the particle  $S$  decays in the second channel ( $S \rightarrow \varphi_2\varphi_2$ ) in the time interval between  $t$  and  $t + dt$  and the integral

$$w_2(t) = \int_0^t du h_2(u) = \sum_{\mathbf{k}} |\langle \varphi_{2,\mathbf{k}}\varphi_{2,-\mathbf{k}} | e^{-iHt} | S \rangle|^2 \quad (84)$$

represents the probability that the particle  $S$  decays into the second channel in the time interval  $(0, t)$ . The equality  $w(t) = w_1(t) + w_2(t)$  holds by construction (see Eq. (24)) and is intuitively clear: the total decay probability between  $(0, t)$  is the sum of the decay probabilities in each channel in the same time interval.

The symbolic expressions for  $h_1(t)$  and  $h_2(t)$  in terms of state vectors are obtained by deriving Eqs. (83) and (84):

$$h_1(t) = \frac{d}{dt} \left( \sum_{\mathbf{k}} |\langle \varphi_{1,\mathbf{k}} \varphi_{1,-\mathbf{k}} | e^{-iHt} | S \rangle|^2 \right), \quad (85)$$

$$h_2(t) = \frac{d}{dt} \left( \sum_{\mathbf{k}} |\langle \varphi_{2,\mathbf{k}} \varphi_{2,-\mathbf{k}} | e^{-iHt} | S \rangle|^2 \right). \quad (86)$$

In this section the decay probability densities  $h_1(t)$  and  $h_2(t)$  are not calculated directly, because the evaluation of the matrix elements  $\langle \varphi_{1,\mathbf{k}} \varphi_{1,-\mathbf{k}} | e^{-iHt} | S \rangle$  and the subsequent partial sum is not an easy task in QFT. We will follow a different way by starting from the decay probability density  $h(t)$ , which by construction is the sum of  $h_1(t)$  and  $h_2(t)$ . It is then possible to postulate the expressions for the latter quantities and then a posteriori verify that they fulfill all the required properties. We will check the numerical validity of our solutions with the help of the QM-LH approach (both in the nonrelativistic and the relativistic frameworks) in Sec. 5.

An important object of interest in this section is the ratio of decay probability densities  $R(t)$  defined as

$$R(t) = \frac{h_1(t)}{h_2(t)}. \quad (87)$$

It represents the ratio of the probabilities that the particle  $S$  decays in the first channel and in the second channel in the time interval between  $t$  and  $t + dt$ . Its study is interesting because, as we shall see,  $R(t)$  shows a peculiar behavior as function of time.

For a better understanding of the presented functions several plots for the numerical values of Eq. (18) are presented.

## 4.2 The partial distributions $d_S^{(1)}(x)$ and $d_S^{(2)}(x)$ and amplitudes $a_1(t)$ and $a_2(t)$

The distribution  $d_S(x)$  can be written as the sum of the two functions  $d_S^{(1)}(x)$  and  $d_S^{(2)}(x)$ :

$$d_S(x) = d_S^{(1)}(x) + d_S^{(2)}(x), \quad (88)$$

with

$$d_S^{(1)}(x) = \frac{2x}{\pi} \lim_{\varepsilon \rightarrow 0} \frac{2g_1^2 \text{Im} [\Sigma(x^2, m_1^2)] + \varepsilon}{(x^2 - M_0^2 + \text{Re} \Pi(x^2))^2 + (\text{Im} \Pi(x^2) + \varepsilon)^2}, \quad (89)$$

$$d_S^{(2)}(x) = \frac{2x}{\pi} \lim_{\varepsilon \rightarrow 0} \frac{2g_2^2 \text{Im} [\Sigma(x^2, m_2^2)] + \varepsilon}{(x^2 - M_0^2 + \text{Re} \Pi(x^2))^2 + (\text{Im} \Pi(x^2) + \varepsilon)^2}. \quad (90)$$

The integrals

$$\int_0^\infty dx d_S^{(1)}(x) \text{ and } \int_0^\infty dx d_S^{(2)}(x) \quad (91)$$

represent the decay fractions, i.e. the probabilities that the particle  $S$  decays in channel 1 or in channel 2 in the time interval  $(0, \infty)$ , respectively [25]. Obviously, their sum is unity in virtue of Eq. (17). Note, in the BW limit the integral  $\int_0^\infty dx d_S^{(i)}(x)$  represents the ratio  $\Gamma_i/\Gamma$ , see Sec. 4.3.5 for details.

The functions  $d_S^{(1)}(x)$  and  $d_S^{(2)}(x)$  have been plotted in Fig. 6 for the numerical values of Eq. (18).

We now introduce the Fourier transforms of  $d_S^{(1)}(x)$  and  $d_S^{(2)}(x)$ :

$$a_1(t) = \int_{-\infty}^\infty dx d_S^{(1)}(x) e^{-ixt}, \quad (92)$$

$$a_2(t) = \int_{-\infty}^{\infty} dx d_S^{(2)}(x) e^{-ixt} . \quad (93)$$

The survival amplitude  $a(t)$  can be rewritten as

$$a(t) = \int_{-\infty}^{\infty} dx d_S(x) e^{-ixt} = \int_{-\infty}^{\infty} dx d_S^{(1)}(x) e^{-ixt} + \int_{-\infty}^{\infty} dx d_S^{(2)}(x) e^{-ixt} = a_1(t) + a_2(t) . \quad (94)$$

Then, the survival probability  $p(t)$  can be expressed as:

$$\begin{aligned} p(t) &= a^*(t)a(t) = (a_1^*(t) + a_2^*(t)) (a_1(t) + a_2(t)) \\ &= a_1^*(t)a_1(t) + a_1^*(t)a_2(t) + a_1(t)a_2^*(t) + a_2^*(t)a_2(t) \\ &= A_1(t) + 2A_{mix}(t) + A_2(t) , \end{aligned} \quad (95)$$

where the three real quantities

$$A_1(t) = |a_1(t)|^2 = \left| \int_{-\infty}^{\infty} dx d_S^{(1)}(x) e^{-ixt} \right|^2 , \quad (96)$$

$$A_2(t) = |a_2(t)|^2 = \left| \int_{-\infty}^{\infty} dx d_S^{(2)}(x) e^{-ixt} \right|^2 , \quad (97)$$

$$A_{mix}(t) = \frac{a_1^*(t)a_2(t) + a_1(t)a_2^*(t)}{2} = \text{Re} [a_1(t)a_2^*(t)] , \quad (98)$$

have been introduced.

Therefore, the decay probability density  $h(t) = -p'(t)$  can be rewritten as:

$$h(t) = -A_1'(t) - 2A_{mix}'(t) - A_2'(t) . \quad (99)$$

This form is the starting point for the postulate about  $h_1(t)$  and  $h_2(t)$  as presented in the next subsection.

### 4.3 The decay probabilities $w_1(t)$ and $w_2(t)$ and the densities $h_1(t)$ and $h_2(t)$ as functions of $a_1(t)$ and $a_2(t)$ : a conjectured solution and its properties

#### 4.3.1 The postulate about $h_i(t)$ and $w_i(t)$

The key functions in the present study are the densities of decay probability per each channel, denoted as  $h_1(t)$  and  $h_2(t)$ , which have been introduced in the formal expressions (85) and (86).

We *postulate* that the functions  $h_1(t)$  and  $h_2(t)$  can be calculated as:

$$h_1(t) = -A_1'(t) - A_{mix}'(t) , \quad (100)$$

$$h_2(t) = -A_2'(t) - A_{mix}'(t) . \quad (101)$$

The direct calculation of Eqs. (85) and (86) is a complicated task in QFT, see also next Section where the explicit evaluation in terms of Lee Hamiltonian(s) is performed. Here we argue that it is possible to express the final result by using the introduced partial amplitudes  $a_1(t)$  and  $a_2(t)$ . Intuitively, we have split Eq. (99) into two pieces by assigning the mixing term  $-2A_{mix}'(t)$  in equal parts to each channels. In the following subsections we show that Eqs. (100)-(101) fulfill all the required properties.

The decay probabilities  $w_1(t)$  and  $w_2(t)$ , formally defined in Eqs. (83) and (84), can be easily obtained from Eqs. (100)-(101) as:

$$w_1(t) = A_1(0) + A_{mix}(0) - A_1(t) - A_{mix}(t) , \quad (102)$$

$$w_2(t) = A_2(0) + A_{mix}(0) - A_2(t) - A_{mix}(t) . \quad (103)$$

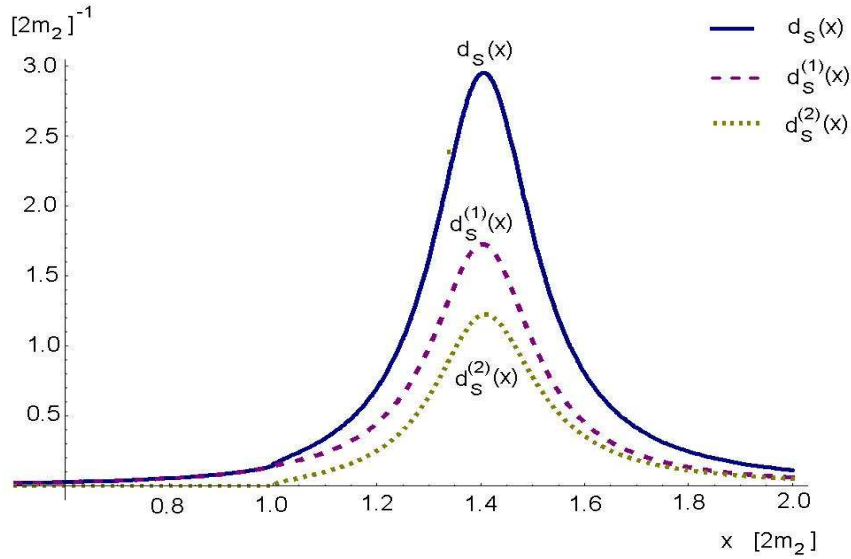


Figure 6: The partial distributions  $d_S^{(1)}(x)$  and  $d_S^{(2)}(x)$  are plotted and compared to  $d_S(x)$ . The numerical values of Eq. (18) are used.

In Fig. 7 the functions  $h_1(t)$  and  $h_2(t)$  as calculated from Eqs. (100)-(101) are plotted for the usual numerical example of Eq. (18) and are compared to  $h(t)$ . Both functions vanish for  $t = 0$  and have a qualitative similar behavior to the sum  $h(t)$ , reaching a maximum for short times and then decreasing later on. It is also interesting to notice that both functions show an oscillating behavior on top of the exponential law.

#### 4.3.2 Sum

The sum  $h_1(t) + h_2(t)$  must obviously give  $h(t)$ :

$$h(t) = h_1(t) + h_2(t) . \quad (104)$$

In fact, the quantity  $h(t)dt$  represents the probability that the particle  $S$  decays between  $t$  and  $t + dt$ , which must be the sum of the probability of decaying into the first channel and into the second channel. This property, which indeed has been our starting point leading to our postulate, is easily verified, see Eq. (99) and Eqs. (100)-(101).

#### 4.3.3 Limits $g_2 \rightarrow 0$ and $g_1 \rightarrow 0$

It is important to check that  $h_1(t)$  and  $h_2(t)$  fulfill the correct limits when one of the coupling constant is sent to zero. In the limit  $g_2 \rightarrow 0$  one has, as expected, that

$$h_1(t) = -A_1'(t) , h_2(t) = 0 . \quad (105)$$

Thus, only the first channel survives and  $h(t) = h_1(t)$ . Similarly, in the limit  $g_1 \rightarrow 0$  one has the specular situation

$$h_2(t) = -A_2'(t) , h_1(t) = 0 . \quad (106)$$

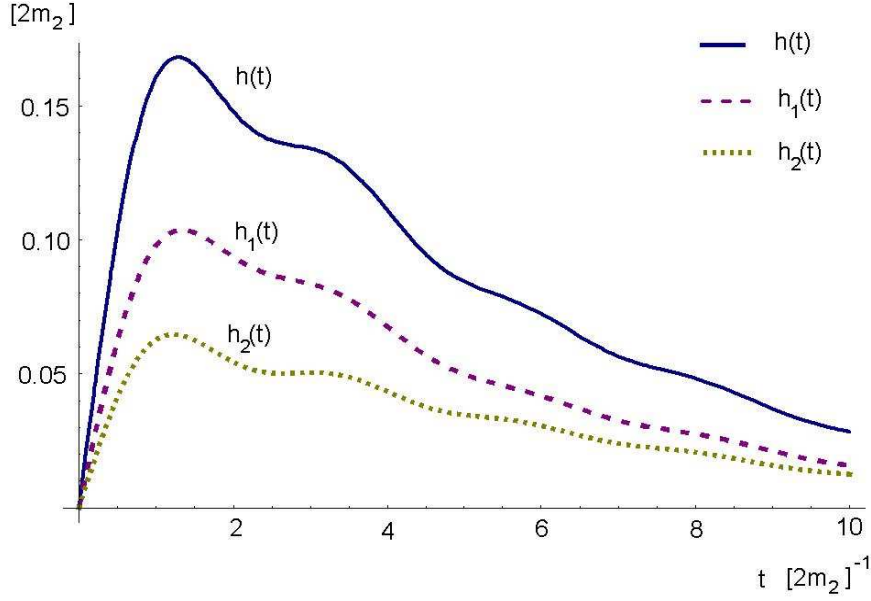


Figure 7: The partial decay probability densities  $h_1(t)$  and  $h_2(t)$  are plotted and compared to  $h(t)$ . The numerical values of Eq. (18) are used.

#### 4.3.4 Integrals and partial decay rates

The functions  $h_1(t)$  and  $h_2(t)$  must fulfill the following requirements:

$$w_1(\infty) = \int_0^\infty dt h_1(t) = \int_0^\infty dx d_S^{(1)}(x) , \quad (107)$$

$$w_2(\infty) = \int_0^\infty dt h_2(t) = \int_0^\infty dx d_S^{(2)}(x) . \quad (108)$$

In fact,  $w_1(\infty) = \int_0^\infty dt h_1(t)$  represents the probability that the particle decays in the first channel between  $(0, \infty)$ , a quantity which is also given by  $\int_0^\infty dx d_S^{(1)}(x)$ . (This is a typical result of the study of line shapes, e.g. Ref. [25] and refs. therein.)

In order to prove Eq. (107) we calculate

$$\int_0^\infty dt h_1(t) = \int_0^\infty dt (-A_1'(t) - A_{mix}'(t)) = A_1(0) + A_{mix}(0) . \quad (109)$$

Taking into account that

$$A_1(0) = \left( \int_{-\infty}^\infty dx d_S^{(1)}(x) \right)^2 , \quad (110)$$

$$A_{mix}(0) = \left( \int_{-\infty}^\infty dx d_S^{(1)}(x) \right) \left( \int_{-\infty}^\infty dx d_S^{(2)}(x) \right) , \quad (111)$$

we obtain:

$$A_1(0) + A_{mix}(0) = \left( \int_{-\infty}^\infty dx d_S^{(1)}(x) \right) \left( \int_{-\infty}^\infty dx d_S^{(1)}(x) + \int_{-\infty}^\infty dx d_S^{(2)}(x) \right) = \int_{-\infty}^\infty dx d_S^{(1)}(x) . \quad (112)$$

In this way Eq. (107) is proven. The validity of Eq. (108) can be easily proven following the same steps.

### 4.3.5 The Breit-Wigner limit

Also in the two-channel case it is important to study the Breit-Wigner limit. The (non-relativistic) BW distributions  $d_{S\text{-BW}}^{(1)}(x)$  and  $d_{S\text{-BW}}^{(2)}(x)$  of Eqs. (89)-(90) are obtained just as in Sec. 2.3:

$$d_S^{(1)}(x) \rightarrow d_{S\text{-BW}}^{(1)}(x) = \frac{\Gamma_1}{2\pi} \frac{1}{(x-M)^2 + \Gamma^2/4} , \quad (113)$$

$$d_S^{(2)}(x) \rightarrow d_{S\text{-BW}}^{(2)}(x) = \frac{\Gamma_2}{2\pi} \frac{1}{(x-M)^2 + \Gamma^2/4} . \quad (114)$$

Obviously,  $d_{S\text{-BW}}(x) = d_{S\text{-BW}}^{(1)}(x) + d_{S\text{-BW}}^{(2)}(x)$ . The amplitudes  $a_1(t)$  and  $a_2(t)$  read in the BW limit

$$a_1(t) \rightarrow a_{1,\text{BW}}(t) = \int_{-\infty}^{\infty} dx d_S^{(1)}(x) e^{-ixt} = \frac{\Gamma_1}{\Gamma} e^{-\Gamma t/2} e^{iMt} , \quad (115)$$

$$a_2(t) \rightarrow a_{2,\text{BW}}(t) = \int_{-\infty}^{\infty} dx d_S^{(2)}(x) e^{-ixt} = \frac{\Gamma_2}{\Gamma} e^{-\Gamma t/2} e^{iMt} . \quad (116)$$

The quantity  $A_1$ ,  $A_2$  and  $A_{\text{mix}}$  take the form

$$A_1(t) \rightarrow A_{1,\text{BW}}(t) = |a_{1,\text{BW}}(t)|^2 = \left(\frac{\Gamma_1}{\Gamma}\right)^2 e^{-\Gamma t} , \quad (117)$$

$$A_2(t) \rightarrow A_{2,\text{BW}}(t) = |a_{2,\text{BW}}(t)|^2 = \left(\frac{\Gamma_2}{\Gamma}\right)^2 e^{-\Gamma t} , \quad (118)$$

$$A_{\text{mix}}(t) \rightarrow A_{\text{mix},\text{BW}}(t) = \frac{a_{1,\text{BW}}^*(t) a_{2,\text{BW}}(t) + a_{1,\text{BW}}(t) a_{2,\text{BW}}^*(t)}{2} = \frac{\Gamma_1 \Gamma_2}{\Gamma^2} e^{-\Gamma t} . \quad (119)$$

Out of these equations we can easily evaluate the functions  $h_1$  and  $h_2$  in the BW limit:

$$h_1 \rightarrow h_{1,\text{BW}}(t) = \left(\frac{\Gamma_1^2}{\Gamma} + \frac{\Gamma_1 \Gamma_2}{\Gamma}\right) e^{-\Gamma t} = \Gamma_1 e^{-\Gamma t} , \quad (120)$$

$$h_2 \rightarrow h_{2,\text{BW}}(t) = \left(\frac{\Gamma_2^2}{\Gamma} + \frac{\Gamma_1 \Gamma_2}{\Gamma}\right) e^{-\Gamma t} = \Gamma_2 e^{-\Gamma t} . \quad (121)$$

The decay probabilities  $w_1(t)$  and  $w_2(t)$  take the form:

$$w_1(t) \rightarrow w_{1,\text{BW}}(t) = \frac{\Gamma_1}{\Gamma} (1 - e^{-\Gamma t}) , \quad (122)$$

$$w_2(t) \rightarrow w_{2,\text{BW}}(t) = \frac{\Gamma_2}{\Gamma} (1 - e^{-\Gamma t}) . \quad (123)$$

In particular, when calculating the decay fractions in a given channel, we obtain the expected results

$$w_{1,\text{BW}}(\infty) = \int_0^{\infty} dt h_{1,\text{BW}}(t) = \frac{\Gamma_1}{\Gamma} , \quad (124)$$

$$w_{2,\text{BW}}(\infty) = \int_0^{\infty} dt h_{2,\text{BW}}(t) = \frac{\Gamma_2}{\Gamma} . \quad (125)$$

In Fig. 8 the functions  $h_1(t)$  and  $h_2(t)$  of Eqs. (100)-(101) are plotted separately and compared to the corresponding exponential functions  $h_{1,\text{BW}}(t)$  and  $h_{2,\text{BW}}(t)$ . It is visible that also in each channel the deviations from the BW limit are not negligible for small times, but become smaller and smaller with increasing  $t$ . It is also interesting to notice that the two functions  $h_1(t)$  and  $h_2(t)$  oscillate around the corresponding BW limit in a different and peculiar way.

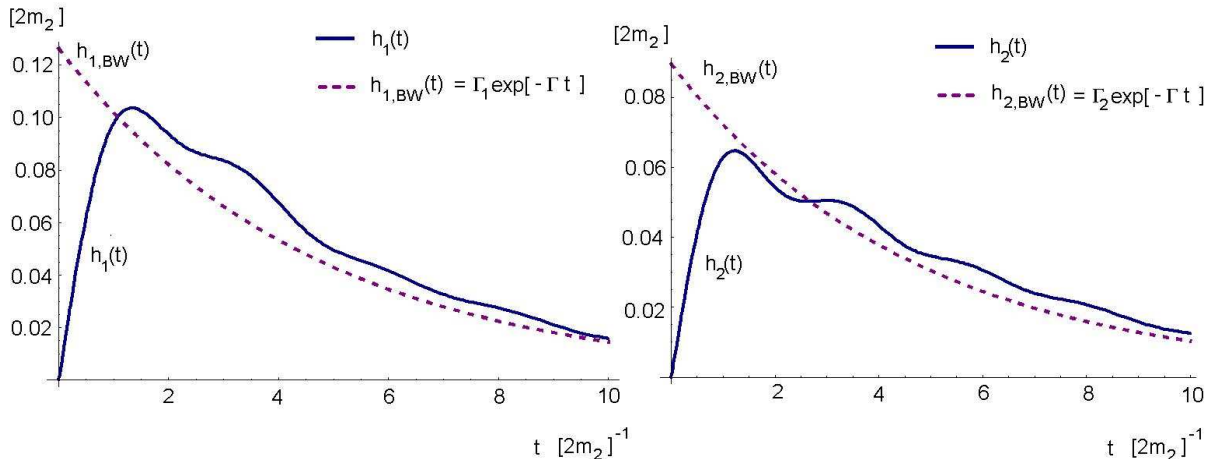


Figure 8: Left: the decay probability density into the first channel  $h_1(t)$  is plotted together with the BW limit  $h_{1,BW}(t) = \Gamma_1 e^{-\Gamma t}$ . Right: the same for  $h_1(t)$  and  $h_{2,BW}(t)$ . In both cases the numerical values of Eq. (18) have been used.

The results obtained in the BW limit are expected: the usual exponential law is recovered and the different channels are proportional to the corresponding partial decay width  $\Gamma_i$ . In the BW limit the ratio  $R(t)$  defined in Eq. (87) becomes a constant:

$$R(t) = \frac{h_1(t)}{h_2(t)} \rightarrow R_{BW}(t) = \frac{\Gamma_1}{\Gamma_2} = \text{const} . \quad (126)$$

This result does not hold true in the general case, in which  $R(t)$  varies with  $t$ . In Fig. 9 the function  $R(t)$  and the constant BW limit  $R_{BW}(t) = \Gamma_1/\Gamma_2$  are shown: the deviation of the exact result  $R(t)$  from the BW limit is sizable. There are time intervals in which the production of  $\varphi_1\varphi_1$  pairs is enhanced with respect to  $\varphi_2\varphi_2$  pairs, and there are time intervals in which the opposite is true. This is an extremely interesting behavior which shall be studied in detail in the future. The reason for the large departure from the constant BW result can be also traced back to the oscillating behavior of both functions  $h_1(t)$  and  $h_2(t)$ . The frequencies of the oscillations are different, and thus the ratio  $R(t)$  results as a complicated outcome. Moreover, the deviations are still large also for large times. This is due to the fact that for  $t \gg \tau_{BW}$  the quantities  $h_1(t)$  and  $h_2(t)$  are both small numbers: even small variations from the exponential limit cause large deviations of the ratio  $R(t)$  from the constant value  $\Gamma_1/\Gamma_2$ . The full study of the large time behavior of the function  $R(t)$  represents also an interesting outlook for future studies.

Finally, in Fig. 10 we plot the ratios

$$\frac{h_i(t)}{h(t)} \text{ and } \frac{w_i(t)}{w(t)} , i = 1, 2 .$$

Both functions tend to the constant value  $\Gamma_i/\Gamma$  in the BW limit. One can see that  $h_i(t)/h(t)$  oscillate and that  $w_i(t)/w(t)$  tend to a constant limit which are not coincident with the naive BW expectations, thus showing that deviations persist also for large times.

#### 4.3.6 Invariance under time-reversal

The underlying theory described by the Lagrangian of Eq. (1) is invariant under time reversal; therefore, the physical quantities under study should also reflect this basic symmetry. The amplitude  $a(t)$

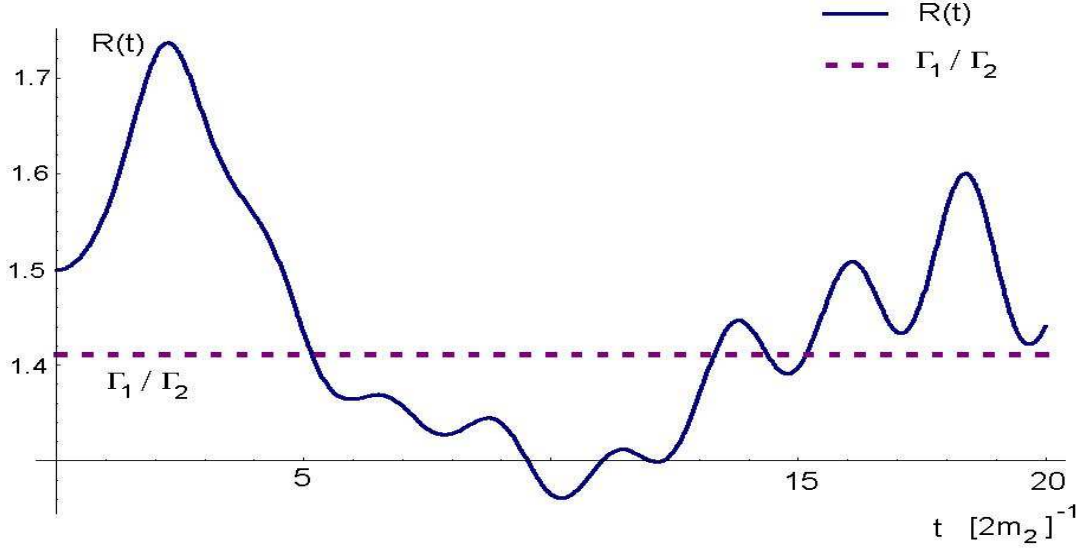


Figure 9: The ratio  $R(t) = h_1(t)/h_2(t)$  (solid line) is plotted and compared to the constant BW limit  $R_{\text{BW}}(t) = \Gamma_1/\Gamma_2$  (dashed line) Large deviations, which persist also at large times, take place. As usual, the numerical values (18) have been used.

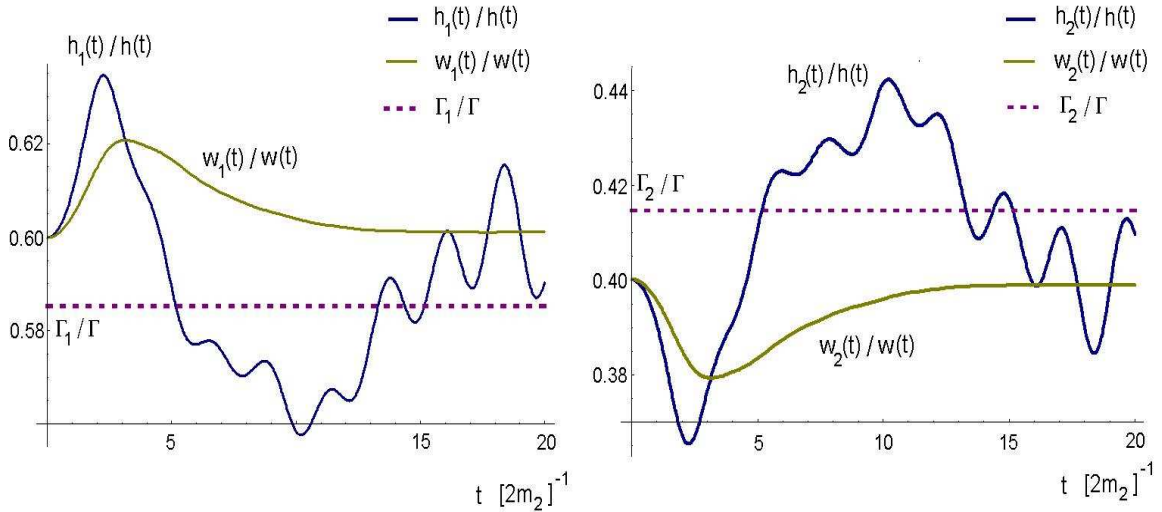


Figure 10: Left:  $h_1(t)/h(t)$  and  $w_1(t)/w(t)$  have been plotted and compared to the constant BW limit  $\Gamma_1/\Gamma$ . Right:  $h_2(t)/h(t)$  and  $w_2(t)/w(t)$  have been plotted and compared to the BW limit  $\Gamma_2/\Gamma$ . The numerical values of Eq. (18) have been used.

defined in Eq. (19) fulfills the equation  $a(-t) = a^*(t)$ . As a consequence, the survival probability  $p(t) = a^*(t)a(t)$  is invariant under time reversal:  $p(-t) = p(t)$ .

Also the decay probability  $w(t)$  in Eq. (24) is invariant under time reversal for the very same reason:  $w(-t) = w(t)$ . Notice that the decay probability density  $h(t)$  is odd under time reversal:  $h(-t) = -h(t)$ . In this way the invariance of the physical quantity  $h(t)dt$ , and therefore  $w(t)$ , is assured.

The invariance under time reversal is satisfied also by the decay probabilities  $w_1(t)$  and  $w_2(t)$ , as the formal expressions in Eqs. (83) and (84) show:  $w_1(-t) = w_1(t)$ ,  $w_2(-t) = w_2(t)$ . Due to the mathematical property  $a_{1,2}(-t) = a_{1,2}^*(t)$  also the expressions for  $w_1(t)$  and  $w_2(t)$  in Eqs. (102) and (103) fulfill the requirement of invariance under time reversal. Just as for the function  $h(t)$ , the decay probability densities  $h_1(t)$  and  $h_2(t)$  must be odd under time reversal:  $h_1(-t) = -h_1(t)$  and  $h_2(-t) = -h_2(t)$ . This is easily verified for Eqs. (100) and (101).

### 4.3.7 On the uniqueness of the postulated solution

Eqs. (100)-(101) fulfill all the required conditions to represent the decay probability densities in the first and the second channel. However, it is important to study the uniqueness of presented solutions.

A different combination  $\tilde{h}_1(t) = -A'_1(t) - \alpha A'_{mix}(t)$ ,  $\tilde{h}_2(t) = -A'_2(t) - \beta A'_{mix}(t)$  with  $\alpha + \beta = 2$  and  $\alpha, \beta \neq 1$  would obviously satisfy the constraint given by the sum (104) (Sec. 4.3.2) and the limits  $g_1, g_2 \rightarrow 0$  (Sec. 4.3.3), but would not fulfill the constraints given by the integrals (107)-(108) and would not reproduce the correct BW limit. Therefore, only the case  $\alpha = \beta = 1$  is allowed.

More in general, one can try to find alternative solutions by writing down the functions

$$\tilde{h}_1(t) = h_1(t) + \delta(t) \quad (127)$$

$$\tilde{h}_2(t) = h_2(t) - \delta(t) \quad (128)$$

where the ‘hypothetical’ function  $\delta(t) \equiv \delta(g_1, m_1, g_2, m_2, t)$  has been introduced. While the sum constraint of Eq. (104) is fulfilled by construction, the function  $\delta(g_1, m_1, g_2, m_2, t)$  must vanish for  $g_1 \rightarrow 0$  and for  $g_2 \rightarrow 0$  (Sec. 4.3.3) and the integral over time must vanish,  $\int_0^\infty \delta(t)dt = 0$ , in order that Eqs. (107)-(108) still hold. Then,  $\delta(t)$  must also vanish in the BW limit to be in agreement with Sec. 4.3.5. Moreover, being  $\tilde{h}_1(t)$  and  $\tilde{h}_2(t)$  positive definite,  $|\delta(t)| \leq h_2(t)$  when  $\delta(t) > 0$  and  $|\delta(t)| \leq h_1(t)$  when  $\delta(t) < 0$ . All these properties are automatically fulfilled by the trivial solution  $\delta(t) = 0$ , but the question is if other possibilities exist.

A further property that  $\delta$  must fulfill is obtained by studying the exchange of the two particles. This operation amounts to exchange  $g_1 \longleftrightarrow g_2$  and  $m_1 \longleftrightarrow m_2$ . While in this case  $h_1 \leftrightarrow h_2$ , it must hold that:

$$\delta(g_1, m_1, g_2, m_2, t) = -\delta(g_2, m_2, g_1, m_1, t) . \quad (129)$$

If we consider, for instance, the function

$$\delta(t) = \delta_0 \frac{d}{dt} \text{Im} [a_1(t)a_2^*(t)] \quad (130)$$

where the constant  $\delta_0$  is small enough to guarantee the semi-positive definiteness of  $\tilde{h}_1(t)$  and  $\tilde{h}_2(t)$ , it is easy to prove that Eq. (130) would actually fulfill all the mentioned properties from Sec. 4.3.2 to Sec. 4.3.5 together with the exchange property of Eq. (129). However, it violates time-reversal, because it is even under switch of  $t$ :  $\delta(-t) = \delta(t)$  (while, as shown in Sec. 4.3.6, the decay probability densities must be odd under time reversal). For this reason the only possibility is  $\delta_0 = 0$ , i.e. the function  $\delta(t)$  vanishes.

This discussion can be generalized. Writing  $\delta(t) = \frac{d}{dt} \Delta(t)$  and making the additional assumption that the function  $\Delta(t)$  can be expressed as  $\Delta(t) = \sum_{i,j} c_{ij} a_i(t)a_j^*(t)$  where the coefficients  $c_{ij}$  are pure numbers, it is not possible to build  $\delta(t)$  such that it is odd under time reversal and at the same time fulfills Eq. (129). This chain of arguments represent a partial proof of the validity of Eqs. (100)-(101).

Summarizing, all these arguments enforce our point of view that the Eqs. (100)-(101), and therefore Eqs. (102)-(103), are the correct answer to the problem. However, the final answer can only be given if one can mathematically prove the validity of the equations (100)-(101) under general assumptions. Presently, we did not achieve this point, which remains an important task for future studies. However, by using the formalism of the Lee Hamiltonians it is possible to find the exact expressions for  $h_i(t)$  and  $w_i(t)$ , which allow for a numerical verification of Eqs. (100)-(101), see Sec. 5.

#### 4.3.8 Generalizations

The present discussion can be easily generalized to the case of a  $n$ -channel decay: this case is discussed in Appendix B. Moreover, the formalism is not restricted to scalar field theories only but can be easily generalized to each QFT Lagrangian.

#### 4.3.9 Deviations from the exponential decay law and measurements

In this work we focus our attention to the undisturbed decay probabilities of the system: after the creation at  $t = 0$  the unstable system  $|S\rangle$  evolves according to the Hamiltonian of the system which control its decay. We do not attempt here to include the measurement into the mathematical treatment. This is surely an interesting subject which is left as an outlook.

This problem has been first investigated in Refs. [1, 29, 30]. In particular, in Ref. [29] it has been pointed out that random measurements occurring with a certain mean frequency  $\nu$  make the decay still appear to be an exponential, even if the frequency is large enough to probe the non-exponential decay time. This is indeed a generalization of the simple discussion of Sec.2.5, where the quantum-Zeno effect has been presented as an outcome of pulsed measurements. It is assumed that the measurement lets the state collapse back into the unstable state  $|S\rangle$ , which also implies a reset of the clock to the initial value of  $t = 0$ . In this framework, the deviations from the exponential decay law studied in this work would manifest in an exponential decay laws with a ratio which can be different from  $\Gamma_1/\Gamma_2$  in dependence of the (mean) frequency of the observations.

On the other hand, future studies in this direction should also take into account the theory of measurement, see Ref. [31] and refs. therein, in which it is shown that the influence of the measurement apparatus and its response time can have a non-negligible effect. As studied also in Refs. [32, 33], the outcome may also depend on the details of the experimental apparatus. A detailed investigation of the ‘collapse’ beyond the simple projection postulate is also an interesting direction of study in connection with non-exponential decay laws. Another interesting line of research is to investigate in more details the problem of sequential decay processes analyzed in Ref. [30] by using the approach described in the present manuscript.

## 5 Two-channel case: QM and link to QFT

### 5.1 Exact determination of the decay probabilities $w_1(t)$ and $w_2(t)$ in QM by using the nonrelativistic LH

We now study the two-channel decay problem in the QM framework by using the Lee Hamiltonian  $H$  introduced in Eq. (49).

Due to the formal analogy of the QM-LH and the QFT approaches, we can repeat here all the steps done in Sec. 4.2 and 4.3 leading to the postulated solutions for  $w_i(t)$  and  $h_i(t)$ . They read:

$$\begin{aligned} w_i(t) &= A_i(0) + A_{mix}(0) - A_i(t) - A_{mix}(t) , \quad h_i(t) = -w_i'(t) , \\ A_i(t) &= |a_i(t)|^2 , \quad A_{mix}(t) = \text{Re} [a_1(t)a_2^*(t)] , \end{aligned} \tag{131}$$

where

$$a_i(t) = \left| \int_{-\infty}^{\infty} dx d_S^{(i)}(x) e^{-ixt} \right|^2, \quad d_S^{(i)}(x) = \frac{1}{\pi} \left| \frac{g_i^2 \text{Im}[\Sigma_i(x)]}{(x - M_0 + \text{Re}[\Pi(x)])^2 + \text{Im}^2[\Pi(x)]} \right|. \quad (132)$$

(See Sec. 3.1 for the definitions of the functions  $\Sigma_i(x)$  and  $\Pi(x)$  in the nonrelativistic QM-LH case).

In the present QM-LH treatment we can calculate *exactly* the functions  $w_i(t)$ . To this end we first write the formal expression for the decay probability  $w_i(t)$  in the  $i$ -th channel:

$$w_i(t) = \int_0^t h_i(u) du = \sum_{\mathbf{k}} |\langle i, \mathbf{k} | e^{-iHt} | S \rangle|^2, \quad i = 1, 2. \quad (133)$$

We thus need to evaluate the matrix element

$$\langle i, \mathbf{k} | e^{-iHt} | S \rangle. \quad (134)$$

Proceeding as in Sec. 3.1 we obtain the following expression:

$$\langle i, \mathbf{k} | e^{-iHt} | S \rangle = \frac{i}{2\pi} g_i \frac{f_i(\mathbf{k})}{\sqrt{V}} \int_{-\infty}^{\infty} dE \frac{G_S(E)}{E - \omega_i(\mathbf{k}) + i\varepsilon}. \quad (135)$$

Introducing the dispersion relation of  $G_S(E)$ , see Eq. (67), and performing the subsequent integral, we arrive at the following equation:

$$\langle i, \mathbf{k} | e^{-iHt} | S \rangle = g_i \frac{f_i(\mathbf{k})}{\sqrt{V}} \int_{-\infty}^{\infty} dx d_S(x) \frac{e^{-i\omega_i(\mathbf{k})t} - e^{-ixt}}{\omega_i(\mathbf{k}) - x}. \quad (136)$$

Using now Eq. (133) we obtain the final, exact expression for  $w_i(t)$  (in the continuous limit) as:

$$w_i^{\text{exact}}(t) = \int \frac{d^3k}{(2\pi)^3} g_i^2 f_i^2(\mathbf{k}) \left| \int_{-\infty}^{\infty} dx d_S(x) \frac{e^{-i\omega_i(\mathbf{k})t} - e^{-ixt}}{\omega_i(\mathbf{k}) - x} \right|^2, \quad h_i^{\text{exact}}(t) = -\frac{dw_i^{\text{exact}}(t)}{dt}. \quad (137)$$

We have now compared the expressions in Eq. (137) and Eqs. (131)-(132) for different parametrizations of the functions  $\omega_i(\mathbf{k})$  and  $f_i(\mathbf{k})$ . In particular, we have used:

- (i) A generalized version of the two-pole model developed in Ref. [4], in which two open channels are included. The numerical values have been varied in order to check dependence on them.
- (ii) Modifications of the two-pole model including energy thresholds.
- (iii) Different choices for the loop functions  $f_i(\mathbf{k})$ .

In all these cases we have verified that the two expressions (137) and (131)-(132) are numerically indistinguishable. All the results obtained in the present QM-LH approach lead us to conclude that the postulated expressions in Eqs. (131)-(132) (which have the same form as the QFT-like expressions in Sec. 4.3) represent –at least– a very good approximation of the exact results. A proof of the complete equivalence (or eventually of the –albeit small– deviations) of these expressions is left for the future. In particular, one should check the validity of the Ansatz in Eqs. (131)-(132) under more complicated circumstances, involving a numerical check over a large range of parameters and with different forms of the functions  $f_i(\mathbf{k})$ .

In the end, it is also important to stress that the qualitative behavior of the functions  $h_i(t)$  and  $R(t)$  as evaluated in the present QM-LH approach is very similar to the plots presented in this manuscript:  $h_i(t)$  vanish for  $t \rightarrow 0$  and then tend to the BW limit for large times. Typical oscillations are present and the ratio  $R(t)$  is varying abruptly as in Fig. 9.

## 5.2 Generalization to the relativistic case and link to QFT

We now study the two-channel problem using the formalism developed in Sec. 3.2, in which a relativistic generalization of the QM-LH approach was developed.

The solutions postulated in Sec. 4.2 and 4.3 takes the following form in the present case:

$$\begin{aligned} w_i(t) &= A_i(0) + A_{mix}(0) - A_i(t) - A_{mix}(t) , \quad h_i(t) = -w_i'(t) , \\ A_i(t) &= |a_i(t)|^2 , \quad A_{mix}(t) = \text{Re} [a_1(t)a_2^*(t)] , \end{aligned} \quad (138)$$

where

$$a_i(t) = \left| \int_{-\infty}^{\infty} dx d_S^{(i)}(x) e^{-ixt} \right|^2 , \quad d_S^{(i)}(x) = \frac{2x}{\pi} \left| \frac{g_i^2 \text{Im} [\Sigma_i(x)]}{(x^2 - M_0^2 + \text{Re}[\Pi(x)])^2 + \text{Im}^2 [\Pi(x)]} \right| . \quad (139)$$

(See Sec. 3.2 for the definitions of the functions  $\Sigma_i(x)$  and  $\Pi(x)$  in the relativistic LH treatment). Note that, when using the identifications of Eqs. (79)-(80), the previous equations coincide with those in Sec. 4.3.

By following the same steps of Sec. 5.1 (that is, taking into account the relativistic form of the propagators) we arrive at the following ‘exact’ expressions for  $w_i(t)$  for the relativistic LH approach:

$$w_i^{\text{exact}}(t) = \int \frac{d^3k}{(2\pi)^3} g_i^2 f_i^2(\mathbf{k}) \left| \int_{-\infty}^{\infty} dx d_S(x) \frac{e^{-i\omega_i(\mathbf{k})t} - e^{-ixt}}{\omega_i^2(\mathbf{k}) - x^2} \right|^2 , \quad h_i^{\text{exact}}(t) = -\frac{dw_i^{\text{exact}}(t)}{dt} . \quad (140)$$

Also in this case we have numerically compared the conjectured solutions of Eqs. (138)-(139) with the exact result in Eq. (140) and found them equal.

In particular, when using the identifications of Eqs. (79)-(80) which lead to a mathematical equivalence of the present LH approach with the QFT model described in Secs. 2 and 4, we have recalculated all the numerical results presented in Figs. 2-10 with the help of the exact expressions in Eq. (140): as expected, no deviation was found. This fact reinforces our point of view that the expressions represent the exact result (or a very accurate approximation of it).

## 6 Conclusions

In this work we have studied the decay law(s) as function of time of an unstable particle  $S$ , which can decay into two (or more) decay channels. We have done this investigation in two different theoretical contexts: using a relativistic quantum field theoretical Lagrangian and using a quantum mechanical approach expressed in terms of a Lee Hamiltonian.

In the first part of the manuscript we have reviewed general properties of the survival probability  $p(t)$  and the decay probability density  $h(t) = -p'(t)$  (Fig. 1-5, Sec. 2 and Sec. 3) for both the QFT and the QM cases: the non-exponential behavior of the survival probability  $p(t)$  for short times, the Breit-Wigner limit leading to the usual exponential decay law, and the quantum Zeno effect have been described. Formally, the QFT and the QM-LH approaches are very similar, the main difference being the presence of relativistic propagator in the former case and nonrelativistic propagators in the latter one. To overcome this difference we have also developed a simple relativistic generalization of the QM-LH approach in which the same equations of the QFT case (can) arise.

In the second part of the manuscript (Secs. 4 and 5) we have concentrated our attention on the peculiarities of the decay into each one of the two (or more) available open channels. In the two-channel case the mathematical expressions for the decay probability densities into each channel,  $h_1(t)$  and  $h_2(t)$ , and of their corresponding integrated quantities  $w_1(t) = \int_0^t du h_1(u)$  and  $w_2(t) = \int_0^t du h_2(u)$  have been discussed. Namely,  $h_i(t)dt$  represents the probability that the unstable particle  $S$  decays

into the  $i$ -th channel between  $t$  and  $t + dt$ , while  $w_i(t)$  represent the probability that the particle decays into the  $i$ -th channel between 0 and  $t$ . Obviously,  $w_1(t) + w_2(t) = 1 - p(t)$ .

In particular, in QFT (Sec. 4) we did not evaluate  $h_i(t)$  and  $w_i(t)$  exactly, but we have postulated a solution (Eqs. (100)-(101) in Sec. 4.3, see also Figs. 7-8). We have shown that the proposed expressions for  $h_i(t)$  and  $w_i(t)$  fulfill all the required properties, but we could prove the mathematical exactness of the results only under a restricted set of hypotheses, see Sec. 4.3.7 and below. We have also shown that the conjectured solutions show strong deviations from the Breit-Wigner limit, in which the decay law is exponential. An important quantity that we have studied is the ratio of probability densities  $R(t) = h_1(t)/h_2(t)$ . While this quantity is constant in the Breit-Wigner limit and equals the ratio of the tree-level decay widths ( $R(t) \rightarrow \Gamma_1/\Gamma_2$ ), it turns out that the full expression is in general not constant and may deviate sizably from the constant limit, see Fig. 9. The functions  $h_i(t)/h(t)$  and  $w_i(t)/w(t)$  show also the peculiar characteristics of the two-channel problem and have been plotted in Fig. 10.

In view of the fact that the conjectured solutions in QFT could not be analytically demonstrated in the general case, we have studied the same problem in the formally very similar (up to the presence of nonrelativistic propagators) approach of a nonrelativistic QM-LH approach. In this case, besides the postulated solutions, it is also possible to derive the *exact* form for the functions  $h_i^{exact}(t)$  and  $w_i^{exact}(t)$ . A numerical analysis was performed in order to show that the proposed solutions  $h_i(t)$  and the exact ones  $h_i^{exact}(t)$  coincide, thus proving that the proposed solutions represent –at least– a very good approximation of the exact results. When studying the relativistic generalization of the Lee Hamiltonian approach, in which the equations can be chosen to coincide with the QFT study, we have once more numerically verified that the expressions postulated in the QFT context are valid: using the very same parameters of Eq. (18) we have checked the correctness of Figs. 2-10.

There are various possible outlooks for the future, which can be divided into mathematical developments and physical applications.

On the mathematical side, one can perform the following studies: (i) Mathematical proof of the correctness of the postulated expressions for  $h_i(t)$  and  $w_i(t)$  presented in Sec. 4.3 in the QFT case. If the proposed solutions are not exact, it would be necessary to investigate why they offer such a good numerical approximation to the problem. In this context, one needs to check the numerical validity of the postulated Ansatz under more general conditions. (ii) Inclusion of higher orders in the calculation of the self-energy diagrams of the QFT case, thus going beyond Fig. 1.b. (iii) Extension to (strictly) renormalizable Lagrangians.

On a phenomenological level various investigations are possible: (i) Study of physical processes in the framework of the Standard Model, where decays of unstable particles into many channels have been observed and precisely measured. To this end the mathematical development of the mathematical outlook (iii) is necessary. (ii) Applications to weak decays (such as electronic capture decays) of atoms. This analysis could be important to study in detail the properties of oscillations such as the ones experimentally found in Ref. [26], see also Ref. [11] for a related theoretical discussion. (iii) Applications to hadron physics: the deviations from the non-exponential law are large in this case [14], although they last very short due to the short-living nature of (most) hadrons. However, deviations from the exponential decay law might be interesting in connection to an expanding gas of hadrons produced in heavy ion collisions [27]. (iv) A peculiar situation takes place when one channel is kinematically not allowed,  $M < 2m_2$ . When  $M$  is just slightly smaller than  $2m_2$ , the finite width of the unstable state  $S$  due to its decay into the first channel allows also the decay into the –nominally forbidden– second one. This situation is physically realized in the case of the scalar mesons  $a_0(980)$  and  $f_0(980)$ , see details in Refs. [16, 19, 25, 28] and refs. therein. The study of the temporal evolution in such a case represents an interesting outlook.

As a last remark, it is conceivable that the decay into different channels can be experimentally studied with the procedure of Ref. [8]; asymmetric barriers should be used, in order to allow for different tunneling probabilities in different directions. Then, it would be possible to test in an experimentally controlled way quantities such as the ratio  $R(t) = h_1(t)/h_2(t)$  described in this work. More in general, in connection with the experiments, one should also go beyond the undisturbed time-evolution of the

system and include the measuring procedure as a part of the physical description of the decay.

**Acknowledgments:** The author thanks Giuseppe Pagliara for cooperation and many valuable discussions on the subject and Thomas Wolkanowski for useful remarks.

## A The loop function

In order to regularize the self-energy diagram of Fig. 1.b we introduce at each vertex the vertex-function  $\tilde{\phi}(q)$ . At the level of the Lagrangian formulation this can be achieved by rendering the Lagrangian nonlocal, see details in Refs. [16, 34] and refs. therein. The integral in Eq. (10) takes the form

$$\Sigma(p^2, m^2) = -i \int \frac{d^4 q}{(2\pi)^4} \frac{\tilde{\phi}(q)^2}{\left[ \left( \frac{p+2q}{2} \right)^2 - m^2 + i\varepsilon \right] \left[ \left( \frac{p-2q}{2} \right)^2 - m^2 + i\varepsilon \right]} . \quad (141)$$

A general property of  $\Sigma(x, m^2)$  follows from the optical theorem:

$$(\sqrt{2}g)^2 \text{Im}[\Sigma(x, m^2)] = x \Gamma^{t-1}(x, m, g) \left[ \tilde{\phi}(q = (0, \mathbf{q})) \right]^2 ,$$

where

$$\mathbf{q}^2 = \frac{x^2}{4} - m^2 . \quad (142)$$

Due to spatial isotropy, the function  $\tilde{\phi}(q = (0, \mathbf{q}))$  must depend on  $\mathbf{q}^2$ .

For a generic  $\tilde{\phi}(q)$ , the tree-level decay width is indeed not given by Eq. (2) but takes the following modified form:

$$\Gamma^{t-1}(x, m, g) \rightarrow \Gamma^{t-1}(x, m, g) \left[ \tilde{\phi}(q = (0, \vec{q})) \right]^2 . \quad (143)$$

When assuming that  $\tilde{\phi}(q) = \tilde{\phi}(\mathbf{q})$  (i.e. when we drop the dependence on  $q^0$ ), we can perform, in the rest frame of the  $S$  particle ( $p = (x, 0)$ ), the integral over  $q^0$  in Eq. (141), obtaining:

$$\Sigma(x^2, m^2) = \int \frac{d^3 q}{(2\pi)^3} \frac{\tilde{\phi}^2(\mathbf{q})}{\sqrt{\mathbf{q}^2 + m^2} (4(\mathbf{q}^2 + m^2) - x^2 - i\varepsilon)} . \quad (144)$$

In this work we make the following simple choice for numerical evaluations:

$$\tilde{\phi}(q) = \tilde{\phi}(\mathbf{q}) = \theta(\Lambda^2 - \mathbf{q}^2) , \quad (145)$$

i.e. we work with a sharp cutoff  $\Lambda$ . (In general, the use of smooth functions affects the results only slightly, thus showing a weak dependence on the adopted vertex function. An explicit calculation has been presented in Ref. [15]). In this case, by performing also the spatial integration we obtain the explicit result:

$$\Sigma(x, m^2) = \frac{-\sqrt{4m^2 - x^2}}{8\pi^2 x} \arctan \left( \frac{\Lambda x}{\sqrt{\Lambda^2 + m^2} \sqrt{4m^2 - x^2}} \right) - \frac{1}{8\pi^2} \log \left( \frac{m}{\Lambda + \sqrt{\Lambda^2 + m^2}} \right) . \quad (146)$$

Following comments are in order:

(i) The imaginary part of the self-energy amplitude  $\text{Im}[\Sigma(x^2, m^2)]$  is zero for  $0 < x < 2m$  and nonzero starting at threshold.

(ii) The real part  $(\sqrt{2}g)^2 \text{Re}[\Sigma(x^2, m^2)]$  is nonzero below and above threshold and depends explicitly on the cutoff  $\Lambda$ .

(iii) For the case  $\tilde{\phi}(q) = \theta(\Lambda^2 - \mathbf{q}^2)$ , the optical theorem takes the form

$$(\sqrt{2}g)^2 \text{Im}[\Sigma(x^2, m^2)] = x\Gamma^{t-1}(x, m, g)\theta\left(\sqrt{\Lambda^2 + m^2} - \frac{x}{2}\right), \quad (147)$$

Besides the additional  $\theta$  function, it does not depend on the cutoff  $\Lambda$ . Note that Eq. (13) in the text is strictly speaking valid only for  $x < 2\sqrt{\Lambda^2 + m_1^2}$ . This condition is numerically met in Fig. 2 and Fig. 6.

(iv) The present choice of  $\tilde{\phi}(q)$  breaks Lorentz invariance. This is here not a problem, because we always work in the rest frame of  $S$ . It is also not difficult to generalize  $\tilde{\phi}(q)$  in order that it is Lorentz invariant and delivers the same results of this paper when the rest frame of  $S$  is considered.

As a last step we turn to the issue of the bare and renormalized masses: in this work we started with the bare mass  $M_0$  entering in the Lagrangian of Eq. (1) and then we derived the renormalized mass  $M$  in Eq. (16), arising upon the inclusion and the resummation of the self-energy diagram of Fig. 1.b. Alternatively, one could have added a counterterm in Eq. (1):

$$\mathcal{L} \rightarrow \mathcal{L} - \frac{1}{2}CS^2 \text{ with } C = R(M_0). \quad (148)$$

In this way the mass equation takes the form

$$M^2 - M_0^2 - C + R(M) = 0 \rightarrow M = M_0 .$$

Clearly, all the physical results of this work would be unaffected by this alternative procedure.

## B The $n$ -channel case

In the  $n$ -channel case the interaction Lagrangian takes the form

$$\mathcal{L}_{int} = \sum_{i=1}^n g_i S \varphi_i^2, \quad (149)$$

where the particle  $\varphi_i$  has a mass  $m_i$ . The spectral function (or mass distribution)  $d_S(x)$  can be decomposed as  $d_S(x) = \sum_{i=1}^n d_S^{(i)}(x)$  with

$$d_S^{(i)}(x) = \frac{2x}{\pi} \lim_{\varepsilon \rightarrow 0} \frac{2g_i^2 \text{Im}[\Sigma(p^2, m_i^2)] + \varepsilon}{(x^2 - M_0^2 + \text{Re}\Pi(x^2))^2 + (\text{Im}\Pi(x^2) + \varepsilon)^2}, \quad \Pi(x) = \sum_{i=1}^n (\sqrt{2}g_i)^2 \Sigma(x^2, m_i^2). \quad (150)$$

We define  $a_i(t)$  as the Fourier transform of  $d_S^{(i)}(x)$ :

$$a_i(t) = \int_{-\infty}^{\infty} dx d_S^{(i)}(x) e^{-ixt} \quad (151)$$

Out of  $a_i(t)$  we define

$$A_i(t) = |a_i(t)|^2, \quad A_{mix,i}(t) = \sum_{j=1, j \neq i}^n \frac{a_i(t)a_j^*(t) + a_i^*(t)a_j(t)}{2}. \quad (152)$$

The probability that the state  $|S\rangle$  decays in the time interval  $(t, t + dt)$  into the  $i$ -th channel reads  $h_i(t)dt$ , where

$$h_i(t) = -A'_i(t) - A'_{mix,i}(t). \quad (153)$$

It is possible to define the  $n(n-1)/2$  ratio functions

$$R_{ij}(t) = \frac{h_i(t)}{h_j(t)} \text{ with } i < j, \quad i, j = 1, \dots, n. \quad (154)$$

In the BW limit one has  $R_{ij}(t) \rightarrow \Gamma_i/\Gamma_j$ , where  $\Gamma_i$  is the tree-level decay width in the  $i$ -th channel. In general, we expect large deviations from the BW limit. Indeed, many unstable particles of the Standard Model decay in more than two channels: the analysis of the temporal behavior can be performed through the formulae derived here. Explicit calculations represent an outlook for the future.

## References

- [1] L. Fonda, G. C. Ghirardi and A. Rimini, Rept. Prog. Phys. **41** (1978) 587.
- [2] B. Misra and E. C. G. Sudarshan, J. Math. Phys. **18** (1977) 756. L. A. Khal'fin, 1957 Zh. Eksp. Teor. Fiz. **33** 1371. (Engl. trans. Sov. Phys. JETP **6** 1053).
- [3] H. Zheng, S. Y. Zhu and M. S. Zubairy, Phys. Rev. Lett. **101** (2008) 200404.
- [4] P. Facchi, H. Nakazato, S. Pascazio Phys. Rev. Lett. **86** (2001) 2699-2703. P. Facchi and S. Pascazio, Fundamental Aspects of Quantum Physics, L. Accardi and S. Tasaki eds., Quantum Probability and White Noise Analysis, Vol. 17, p. 222 (2003), arXiv:quant-ph/0202127.
- [5] P. Facchi and S. Pascazio, Phys. Lett. A **241** (1998) 139 [arXiv:quant-ph/9905017]. H. Nakazato, M. Namiki and S. Pascazio, International Journal of Modern Physics B, Volume 10, Issue 03, pp. 247-295 (1996), arXiv:quant-ph/9509016.
- [6] A. P. Balachandran and S. M. Roy, Phys. Rev. Lett. **84** (2000) 4019 [arXiv:quant-ph/9909056]. T. Jittoh, S. Matsumoto, J. Sato, Y. Sato, K. Takeda, Phys. Rev. A **71** (2005) 012109 [quant-ph/0408149]. U. G. Aglietti, P. M. Santini, [arXiv:1010.5926 [quant-ph]].
- [7] W. M. Itano, D. J. Heinzen, J. J. Bollinger and D. J. Wineland, Phys. Rev. A **41** (1990) 2295.
- [8] S. R. Wilkinson, C. F. Bharucha, M. C. Fischer, K. W. Madison, P. R. Morrow, Q. Niu, B. Sundaram, M. G. Raizen Nature **387**, 575 (1997).
- [9] M. C. Fischer, B. Gutiérrez-Medina and M. G. Raizen, Phys. Rev. Lett. **87**, 040402 (2001).
- [10] P. Facchi, S. Pascazio, Phys. Lett. **A241** (1998) 139-144. [quant-ph/9905017].
- [11] F. Giacosa, G. Pagliara, [arXiv:1110.1669 [nucl-th]]. F. Giacosa and G. Pagliara, to appear in the Proceedings of the "50th International Winter Meeting on Nuclear Physics", 23-27 January 2012, Bormio, Italy, arXiv:1204.1896 [nucl-th].
- [12] T. D. Lee, Phys. Rev. **95** (1954) 1329-1334.
- [13] C. B. Chiu, E. C. G. Sudarshan and G. Bhamathi, Phys. Rev. D **46** (1992) 3508.
- [14] F. Giacosa and G. Pagliara, Mod. Phys. Lett. **A26** (2011) 2247-2259. [arXiv:1005.4817 [hep-ph]].
- [15] G. Pagliara, F. Giacosa, Acta Phys. Polon. Supp. **4** (2011). [arXiv:1108.2782 [hep-ph]].
- [16] F. Giacosa and G. Pagliara, Phys. Rev. C **76** (2007) 065204 [arXiv:0707.3594 [hep-ph]].
- [17] N. N. Achasov and A. V. Kiselev, Phys. Rev. D **70** (2004) 111901 [arXiv:hep-ph/0405128].
- [18] H. Nakazato and S. Pascazio, Mod. Phys. Lett. A **10**, 3103 (1995).
- [19] C. Amsler and N. A. Tornqvist, Phys. Rept. **389**, 61 (2004). E. Klempt and A. Zaitsev, Phys. Rept. **454** (2007) 1
- [20] R. F. Alvarez-Estrada, J. L. Sanchez-Gomez, Phys. Lett. **A253** (1999) 252-258. R. F. Alvarez-Estrada, J. L. Sanchez-Gomez, [quant-ph/9807084].

- [21] C. Bernardini, L. Maiani, M. Testa, Phys. Rev. Lett. **71** (1993) 2687-2690. L. Maiani and M. Testa, Annals Phys. **263** (1998) 353 [arXiv:hep-th/9709110].
- [22] E. Witten, Nucl. Phys. B **160** (1979) 57. G. 't Hooft, Nucl. Phys. B **72** (1974) 461.
- [23] F. Giacosa, Phys. Rev. D **80** (2009) 074028 [arXiv:0903.4481 [hep-ph]].
- [24] S. Kamefuchi, L. O'Raiheartaigh and A. Salam, Nucl. Phys. **28** (1961) 529.
- [25] F. Giacosa and G. Pagliara, Nucl. Phys. A **812** (2008) 125 [arXiv:0804.1572 [hep-ph]]. F. Giacosa and G. Pagliara, PoS C **ONFINEMENTS** (2008) 163 [arXiv:0812.3357 [hep-ph]]. D. Black, M. Harada and J. Schechter, Phys. Rev. D **73** (2006) 054017 [arXiv:hep-ph/0601052].
- [26] Y. A. Litvinov, F. Bosch, N. Winckler, D. Boutin, H. G. Essel, T. Faestermann, H. Geissel, S. Hess *et al.*, Phys. Lett. **B664** (2008) 162-168. [arXiv:0801.2079 [nucl-ex]].
- [27] Q. Li, M. Bleicher, J. Phys. G **G36** (2009) 015111. [arXiv:0808.3457 [nucl-th]].
- [28] V. Baru, J. Haidenbauer, C. Hanhart, A. E. Kudryavtsev, U. -G. Meissner, Eur. Phys. J. **A23** (2005) 523-533. [nucl-th/0410099]. F. Giacosa, G. Pagliara, Nucl. Phys. **A833** (2010) 138-155. [arXiv:0905.3706 [hep-ph]]. Y. Kalashnikova, A. E. Kudryavtsev, A. V. Nefediev, J. Haidenbauer, C. Hanhart, Phys. Rev. **C73** (2006) 045203. [nucl-th/0512028].
- [29] A. Degasperis, L. Fonda and G. C. Ghirardi, Nuov. Cim. **21** 471 (1974).
- [30] L. Fonda, G. C. Ghirardi, C. Omero, A. Rimini and T. Weber, Phys. Rev. D **18** (1978) 4757.
- [31] K. Koshino, A. Shimizu, Phys. Rep. **412**, 191 (2005).
- [32] M. Hotta and M. Morikawa, Phys. Lett. A **326**, Issue 1-2, p. 32-41.
- [33] F. Delgado, J. G. Muga, and G. Garcia-Calderon, Phys. Rev. A **74**, 062102 (2006).
- [34] J. Terning, Phys. Rev. D **44** (1991) 887. G. V. Efimov and M. A. Ivanov, "The Quark confinement model of hadrons," *Bristol, UK: IOP (1993) 177 p.* Y. V. Burdanov, G. V. Efimov, S. N. Nedelko and S. A. Solunin, Phys. Rev. D **54** (1996) 4483 [arXiv:hep-ph/9601344]. A. Faessler, T. Gutsche, M. A. Ivanov, V. E. Lyubovitskij and P. Wang, Phys. Rev. D **68** (2003) 014011 [arXiv:hep-ph/0304031]. F. Giacosa, T. Gutsche and A. Faessler, Phys. Rev. C **71** (2005) 025202 [arXiv:hep-ph/0408085].